NUWC-NPT Technical Report 11,799
30 March 2007

Deployable Air Beam Fender System (DAFS): Energy Absorption Performance Analysis

Paul V. Cavallaro
Ranges, Engineering, and Analysis Department

NAVSEA WARFARE CENTERS
NEWPORT

Naval Undersea Warfare Center Division Newport, Rhode Island

PREFACE

This report was funded under NUWC Division Newport Assignment Number TD0207, principal investigator Paul V. Cavallaro (Code 70T). The research was conducted in support of the Center of Excellence for Inflatable Composite Structures at the U.S. Army Natick Soldier Center (NSC) in Natick, MA, through Military Interagency Purchase Request Number 7BDAVN0149. The NSC project officer is Claudia J. Quigley.

The technical reviewer for this report was Andrew J. Hull (Code 8212).

Reviewed and Approved: 30 March 2007

Harriet L. Coleman

Harriet L. Coleman
Head, Ranges, Engineering, and Analysis Department

REPORT DOCUMENTATION PAGE

Form Approved
OMB No. 0704-0188

1. AGENCY USE ONLY *(Leave blank)*

2. REPORT DATE
30 March 2007

3. REPORT TYPE AND DATES COVERED

4. TITLE AND SUBTITLE

Deployable Air Beam Fender System (DAFS): Energy Absorption Performance Analysis

5. FUNDING NUMBERS

6. AUTHOR(S)

Paul V. Cavallaro

7. PERFORMING ORGANIZATION NAME(S) AND ADDRESS(ES)

Naval Undersea Warfare Center Division
1176 Howell Street
Newport, RI 02841-1708

8. PERFORMING ORGANIZATION REPORT NUMBER

TR 11,799

9. SPONSORING/MONITORING AGENCY NAME(S) AND ADDRESS(ES)

U.S. Army Natick Soldier Center
Kansas Street
Natick, MA 01760-5018

10. SPONSORING/MONITORING AGENCY REPORT NUMBER

11. SUPPLEMENTARY NOTES

12a. DISTRIBUTION/AVAILABILITY STATEMENT

Approved for public release; distribution is unlimited.

12b. DISTRIBUTION CODE

13. ABSTRACT (Maximum 200 words)

Performance curves detailing the energy absorption parameters of selectively sized deployable air beam fender systems (DAFSs) were established to enable future efficiencies in fender design. Numerical solutions were generated using the ABAQUS/Explicit Finite Element Analysis (FEA) Program for two mooring configurations: ship-to-ship and ship-to-causeway (non-ballasted). The governing energy balance was presented and the contributions of strain energy and air compressibility were assessed for various inflation pressures and DAFS sizes. The applicability and limitations of analytical methods based on assumptions of material inextensibility were also discussed. Comparisons were made between the numerical and analytical methods to demonstrate the importance of admitting strain energies of the fender material in the energy balance. Equations and conditions for proper scaling of pressure and volume terms in energy absorption calculations were developed and discussed.

14. SUBJECT TERMS

Undersea Warfare	Sea-Basing Operations	Inflated Structures
Air Beams	Fenders	Explicit Methods
Finite Element Analysis	Energy Absorption	Material Extensibility

15. NUMBER OF PAGES
48

16. PRICE CODE

17. SECURITY CLASSIFICATION OF REPORT	18. SECURITY CLASSIFICATION OF THIS PAGE	19. SECURITY CLASSIFICATION OF ABSTRACT	20. LIMITATION OF ABSTRACT
Unclassified	Unclassified	Unclassified	SAR

NSN 7540-01-280-5500

Standard Form 298 (Rev. 2-89)
Prescribed by ANSI Std. Z39-18
298-102

TABLE OF CONTENTS

LIST OF ILLUSTRATIONS

LIST OF ILLUSTRATIONS (Cont'd)

Figure **Page**

LIST OF ILLUSTRATIONS (Cont'd)

Figure **Page**

LIST OF TABLES

LIST OF ABBREVIATIONS, ACRONYMS, AND SYMBOLS

$Area_{contact}$	Surface area of fender contact region
c_p	Specific heat at constant pressure
c_v	Specific heat at constant volume
D	Fender diameter
DAFS	Deployable air beam fender system
E	Elastic modulus
$E_{dissipative\_energy}$	Viscous dissipation energy
$E_{internal\_energy}$	Internal energy
$E_{kinetic\_energy}$	Kinetic energy
EOS	Equation of state
E_{strain_energy}	Strain energy
F	Magnitude of the impact force
FEA	Finite element analysis
JHSV	Joint high-speed vessel
$L_{contact}$	Length of contact surface
$L_{cylinder}$	Length of straight cylindrical fender section
L_o	Fender overall length
Mpsi	Million pounds per square inch
n	Ratio of specific heats
NSC	U.S. Army Natick Soldier Center
NUWC	Naval Undersea Warfare Center
P	Inflation pressure
P_A	Ambient pressure
P_{abs}	Absolute pressure
$PV\text{-}work$	Air compressibility
r	Radius of cylinder
R	Ideal gas constant for air
$\widetilde{R}$	Universal gas constant
V	Internal air volume
$W_{contact}$	Width of contact surface
δ	Displacement along the direction of the impact force vector
θ	Current temperature
θ^Z	Absolute zero temperature
ν	Poisson's ratio
ρ	Density of air

DEPLOYABLE AIR BEAM FENDER SYSTEM (DAFS): ENERGY ABSORPTION PERFORMANCE ANALYSIS

INTRODUCTION

PURPOSE

The deployable air beam fender system (DAFS)[1] was developed to improve sea-basing operations between military surface vessels and marine infrastructures. Based on innovative inflatable-fabric-structures technology, DAFS offers key operational advantages over conventional pneumatic and foam-filled ship fenders: rapid deployment, minimal weight and stowage volume, and selective ballasting controls. DAFS was designed to be organic to the joint high-speed vessel (JHSV); its major performance requirements included (1) sustained functionality up through sea state 3; (2) integrated control system for remote deployment, inflation, ballasting, and retrieval operations; (3) vertical positioning controls; and (4) pressure-relief mechanisms to guard against excessive hull contact pressures. This report documents a study whose goal was to establish fender performance curves for additional DAFS sizes and inflation pressures for ship-to-ship and ship-to-causeway (non-ballasted for this study) impact configurations.

DAFS DEVELOPMENT

DAFS was designed as a vertical fendering system to support two mooring configurations—ship-to-ship and ship-to-causeway (see figures 1 and 2). For the ship-to-ship configuration, DAFS is positioned above the waterline, is generally compressed along its full length, and is filled with air only. In the ship-to-causeway configuration, only part of the DAFS contacts the causeway (or smaller vessel); DAFS may be partially submerged through an automatic ballasting mode to improve positional stability and to prevent causeway override—an event in which the relative motions between vessel and causeway force the fenders out of position and onto the causeway deck, leaving the vessel exposed to direct and potentially damaging impacts.

The main energy-absorbing component of DAFS is the flexible cylindrical pressure vessel (figure 3), which is constructed of a woven, coated fabric with hemispherical ends and is enclosed in an outer layer of urethane. The urethane layer protects the fabric from potential abrasion damage and, because of its low coefficient-of-friction, minimizes the transfer of shearing forces between the ship and fender during impacts. During the development of the DAFS, structural models were generated using the ABAQUS/Explicit finite element analysis (FEA) code[2] to optimize the DAFS design and to predict its energy absorption performance. Quarter-scale and full-scale models were evaluated and compared to prototype tests for a variety of inflation pressures, impact berthing conditions, and ballast levels.[1] Model predictions were validated with correlated test data. The explicit FEA method captured the nonlinearities arising from air compressibility, large deformations, contact, and localized wrinkling. Scalability of the predicted energy absorptions on air volume was also confirmed.

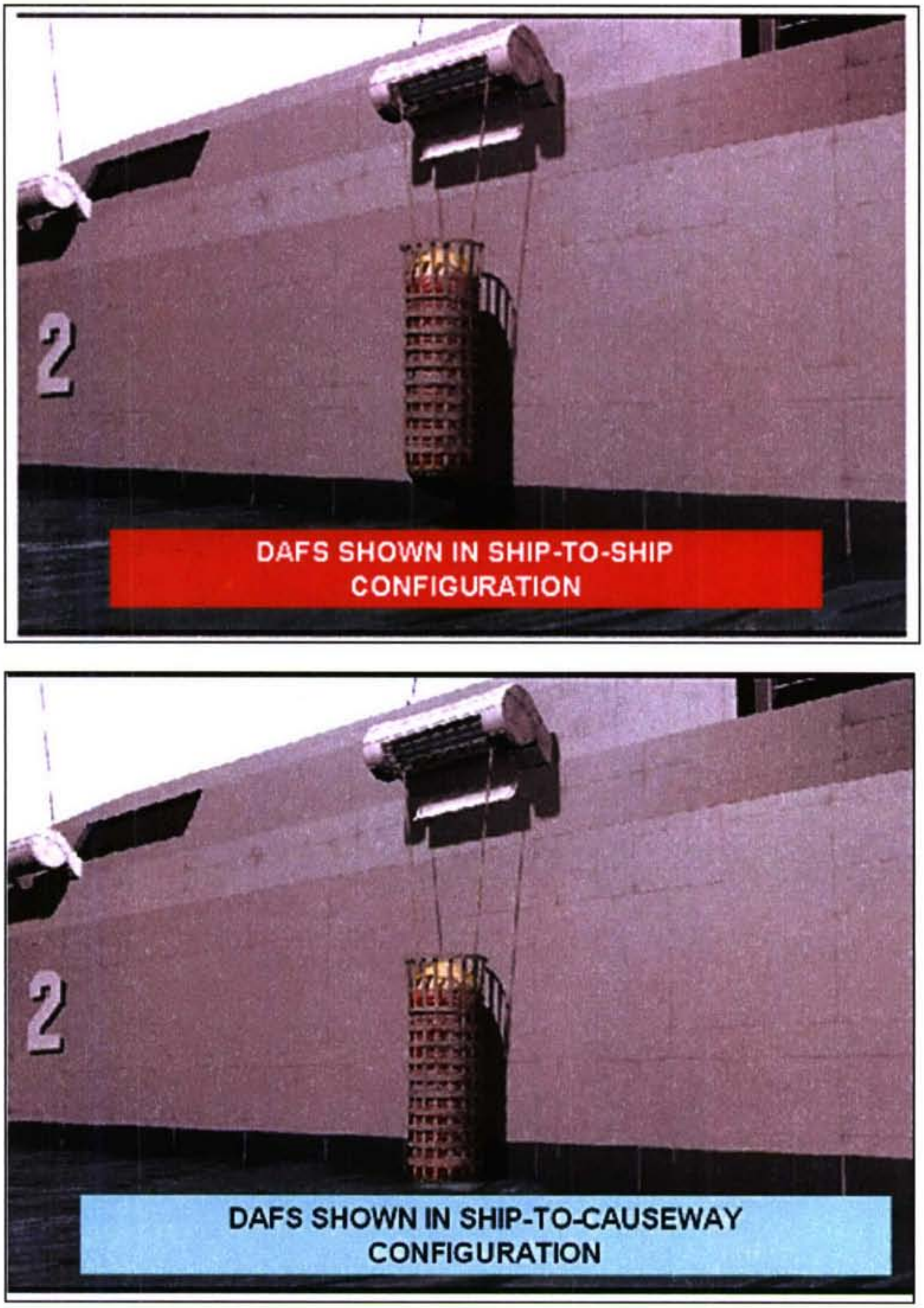

Figure 1. DAFS Mooring Configurations: Ship-to-Ship and Ship-to-Causeway

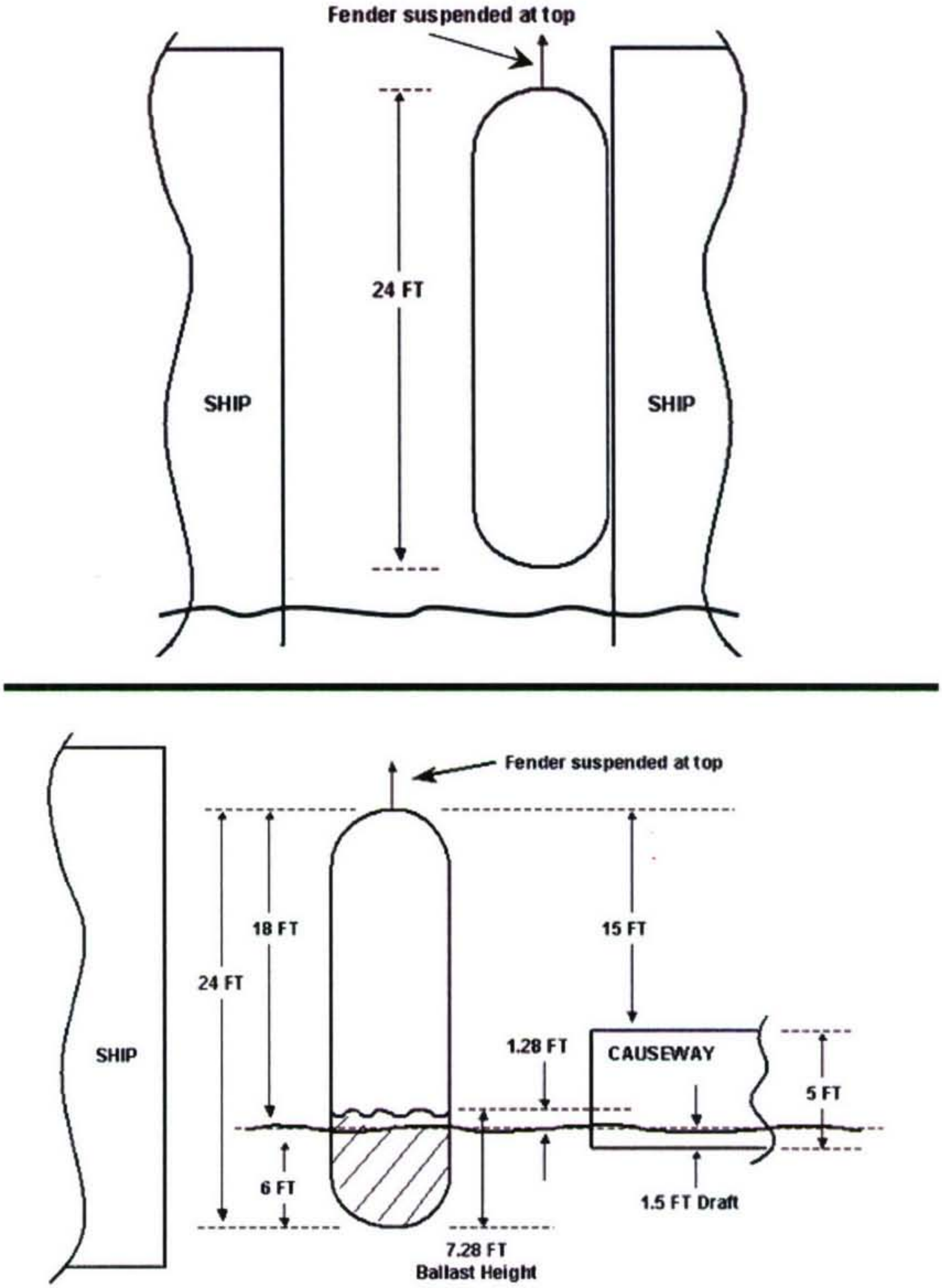

Figure 2. Ship-to-Ship Mooring Configuration (top) and Ship-to-Causeway (bottom) Mooring Configuration for 8-ft-Diameter, 24-ft-Long DAFS Fender

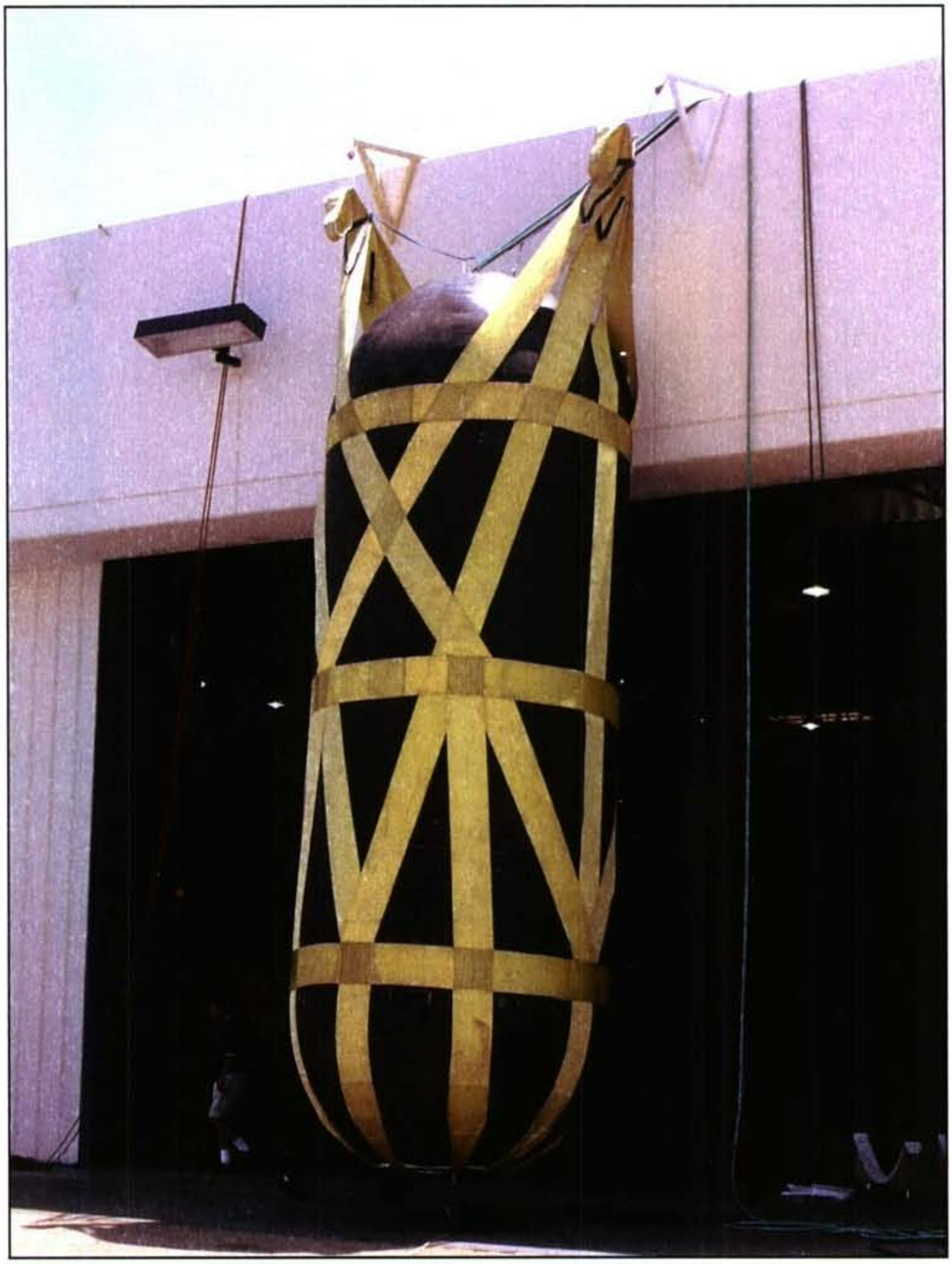

Figure 3. DAFS Prototype (8-ft Diameter, 24-ft Length) with Suspension Lines (Abrasion Layer Not Shown)

GOVERNING ENERGY BALANCE EQUATION

The energy balance equation (equation (1)) that governs DAFS behavior during impact relates the total work done by the external impact force acting on the fender body $\int F\,d\delta$ to the internal energy of the DAFS. The internal energy, $E_{internal\_energy}$, consists of several energy contributions: *PV-work* (air compressibility), strain energy, kinetic energy, and viscous dissipation (damping) energy (strain, kinetic, and viscous dissipation energy contributions pertain to the fabric only). The energy balance equation (equation (1)) is written as:

$$\int F\,d\delta = E_{internal\_energy} = E_{strain\_energy} + E_{kinetic\_energy} + \left(P\int dV + V\int dP\right) + E_{dissipative\_energy}, \qquad (1)$$

where F is the magnitude of the impact force, δ is the displacement along the direction of the impact force vector, P is the air-inflation pressure expressed in gage units, and V is the internal air volume.

For static applications involving appreciable volume changes, the dominant term is the energy absorbed through *PV-work*, namely, $\left(P\int dV + V\int dP\right)$, followed by E_{strain_energy}. The $E_{kinetic\_energy}$ and $E_{dissipative\_energy}$ terms are ideally zero for static events.

ANALYTICAL SOLUTIONS

Analytical solutions of fender energy absorption, such as the one presented in the appendix, are commonly derived by using assumptions of material inextensibility ($E_{strain\_energy} = 0$) in such a way that *PV-work* is the only energy-absorbing means of the fender. By invoking material inextensibility, equations that relate impact displacements to deformed air volumes for limited contact configurations may be readily derived. Analytical solutions are often restricted to those fender impacts in which the deformed air volumes can be completely described as functions of impact displacements (as in the ship-to-ship case with parallel contact surfaces).

Such functions are not easily derived for ship-to-causeway configurations because the volume deformations outside the partial contact region (shown in figure 4) are often difficult to describe analytically. Nonlinear numerical methods including FEA, however, can provide solutions for ship-to-causeway moorings. A comparison of the predicted energy absorptions obtained using the analytical solution in the appendix versus the FEA solution revealed that the analytical solution will underestimate the total work done and overestimate the impact force because it neglects E_{strain_energy}.

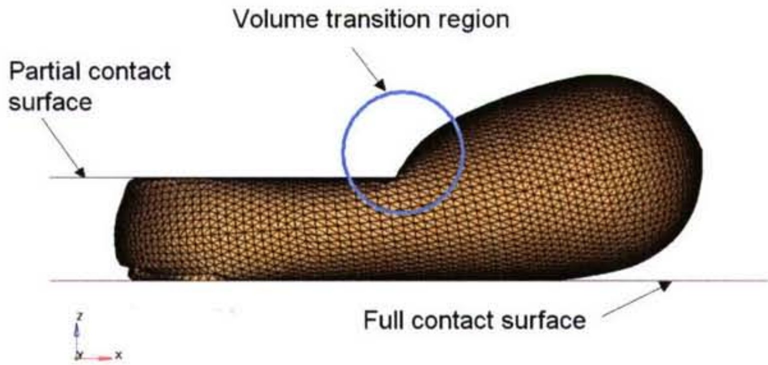

Figure 4. Volume Transition Region Resulting from a Partial (Semi-Infinite) Contact Surface in the Ship-to-Causeway Mooring Configuration

The analytical solution discussed in the appendix can also be used for water-ballasted fenders, provided that the air volumes are known and that the ship-to-ship loading configuration is maintained. Because water is incompressible and if the work done in changing the height of the ballast free-surface during impact can be neglected, the energy absorbed by the fender is assumed to be completely stored as *PV-work*.

NUMERICAL (FEA) MODELS

DESCRIPTION

The DAFS geometries evaluated in this study were cylindrically shaped with hemispherical end caps and a constant overall length-to-diameter ratio (L_o/D) equal to 3.0. Fender diameters were 2, 4, 6, and 8 feet with respective lengths of 6, 12, 18, and 24 feet. Membrane elements were used to represent the fabric material, which was idealized as incapable of developing bending strain energy. The membrane elements, however, admitted extensional and shearing strain energies. The constitutive behavior of the fabric material was assumed to be linearly elastic and isotropic. For each model, the prescribed fabric thickness was 0.005 inch, the elastic modulus E was 0.1 Mpsi, and Poisson's ratio ν was set to 0.3. The DAFS' urethane abrasion layer was considered nonstructural and was not included in the models.

An ideal gas equation of state (EOS) was used to model the internal air as a compressible (pneumatic) fluid as shown in equation (2). The air was assumed to compress adiabatically (that is, no heat transfer was permitted across the fabric boundaries).

$$P + P_A = \rho R\left(\theta - \theta^Z\right), \tag{2}$$

where P_A is the ambient pressure, ρ is the density, R is the ideal gas constant, θ is the current temperature, and θ^z is the absolute zero temperature.

The ideal gas constant R was given by

$$R = \frac{\widetilde{R}}{M_W}, \tag{3}$$

where $\widetilde{R}$ is the universal gas constant, and M_W is the molecular weight.

The relationship of equation (4) can be used to describe the pressure-volume behavior of an ideal gas at two states:

$$\left(P_{abs}V\right)^n_{initial} = \left(P_{abs}V\right)^n_{final}, \tag{4}$$

where n is the ratio of specific heats c_p/c_v (for air, $n = 1.4$), and P_{abs} is the absolute air pressure equal to $P + P_A$.

To correctly model the fluid/structure interaction of the internal air and surrounding fabric, a pressurized cavity was defined along the inside surface of the fabric material. The cavity and its enclosed surface were (1) used to apply the internal pressure directly to the membrane (fabric) elements, (2) used to define the volume of air contained by the cavity in the fender, and (3) coincident with the membrane elements.

Half-symmetry displacement boundary conditions were used to minimize solution times without loss of accuracy for static models; therefore, only one-half of the fender had to be meshed, as shown in figure 5. Nodes located on the plane of symmetry (XZ-plane) were allowed to translate within the plane only (that is, not across the plane). Adjustments were made during postprocessing to reflect results for the full fender. The central node of the top hemispherical end cap was used as the single suspension point and was constrained from moving along the X-axis.

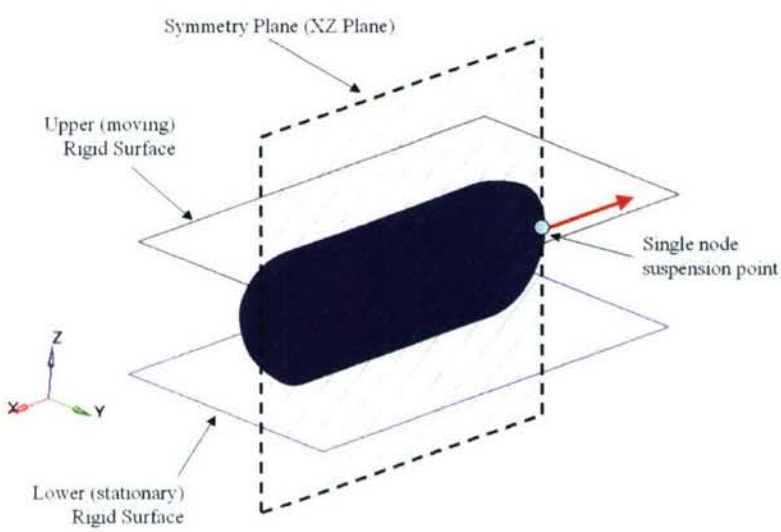

Figure 5. Half-Symmetry DAFS Fender Model

A two-step, quasi-static loading process was used. In step 1, the fender was inflated to the specified inflation pressure and the acceleration caused by gravity (386.4 in./s^2) was applied along the X-axis during a 1.0-second time interval to account for weight as a body force. Inflation pressures considered were 1.5, 2.5, and 5.0 psi. At the end of step 1, the X-direction reaction force at the constrained end cap node was equal to the fender weight.

In step 2, the fender was compressed between two parallel rigid surfaces to approximately 50% of the inflated diameter in a 5.0-second time interval. The bottom rigid surface remained stationary while the top rigid surface displaced vertically downward along the +Z-axis. For the ship-to-ship case, the rigid plates were sized so that, upon 100% diametral compression, full contact over the entire DAFS length would occur. For the ship-to-causeway case, the stationary surface provided full contact at 100% diametral compression while the moving surface projected along only one-half of the DAFS length. The time-histories of pressure, volume, impact force, displacement and energy terms were tracked.

RESULTS

Figures 6 and 7 are displacement contour plots of the ship-to-ship (figure 6) and ship-to-causeway (figure 7) models with an initial inflation pressure of 2.5 psi and deformed to approximately 50% diametral compression. Wrinkling within the hemispherical end caps was observed in the 2-, 4-, and 6-foot-diameter ship-to-ship models for the pressures considered (except for the 6-foot-diameter DAFS inflated to 5 psi); the wrinkling was, however, less pronounced with increasing diameter and pressure. No wrinkling was observed in the 8-foot-diameter *ship-to-ship* models for a minimum pressure of 1.5 psi. Wrinkling occurred at the compressed end cap in each of the ship-to-causeway models.

Figures 8 through 15 show tracked results for the ship-to-ship models (figures 8 through 11) and ship-to-causeway models (figures 12 through 15) for initial inflation pressures of 2.5 psi. Postprocessing operations were performed on the tracked results for each inflation pressure and DAFS diameter—the results of which are shown in the fender performance graphs in figures 16 through 30 for ship to-ship models and in figures 31 through 45 for ship-to-causeway models. These graphs include normalized curves of volume, pressure, impact force, and work done (total energy absorbed). Coefficients were obtained for fifth-order polynomial equations fitting the corresponding performance curves for each diameter and inflation pressure as shown. These equations were provided for future design purposes and can be used to expand the applicability of DAFS fenders to vessels beyond the JHSV. The tracked results and fender performance parameters for both mooring configurations are summarized in tables 1 and 2.

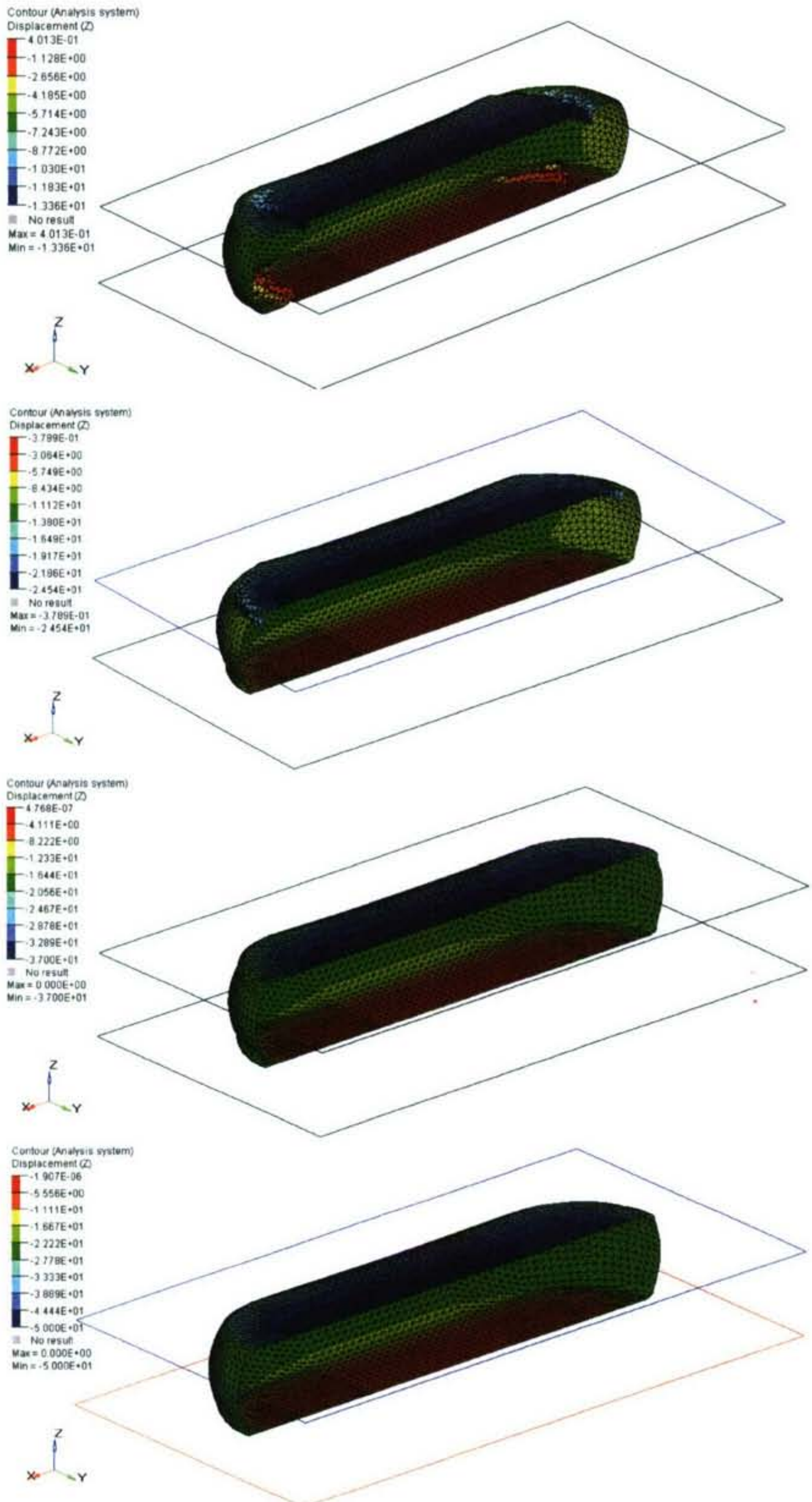

2-ft diameter,
6-ft length

4-ft diameter,
12-ft length

6-ft diameter,
18-ft length

8-ft diameter,
24-ft length

Figure 6. Displacement Contour Plots of 2-, 4-, 6-, and 8-ft-Diameter, Half-Symmetry, Ship-to-Ship Models at Approximately 50% Diametral Compression and 2.5-psi Inflation Pressure

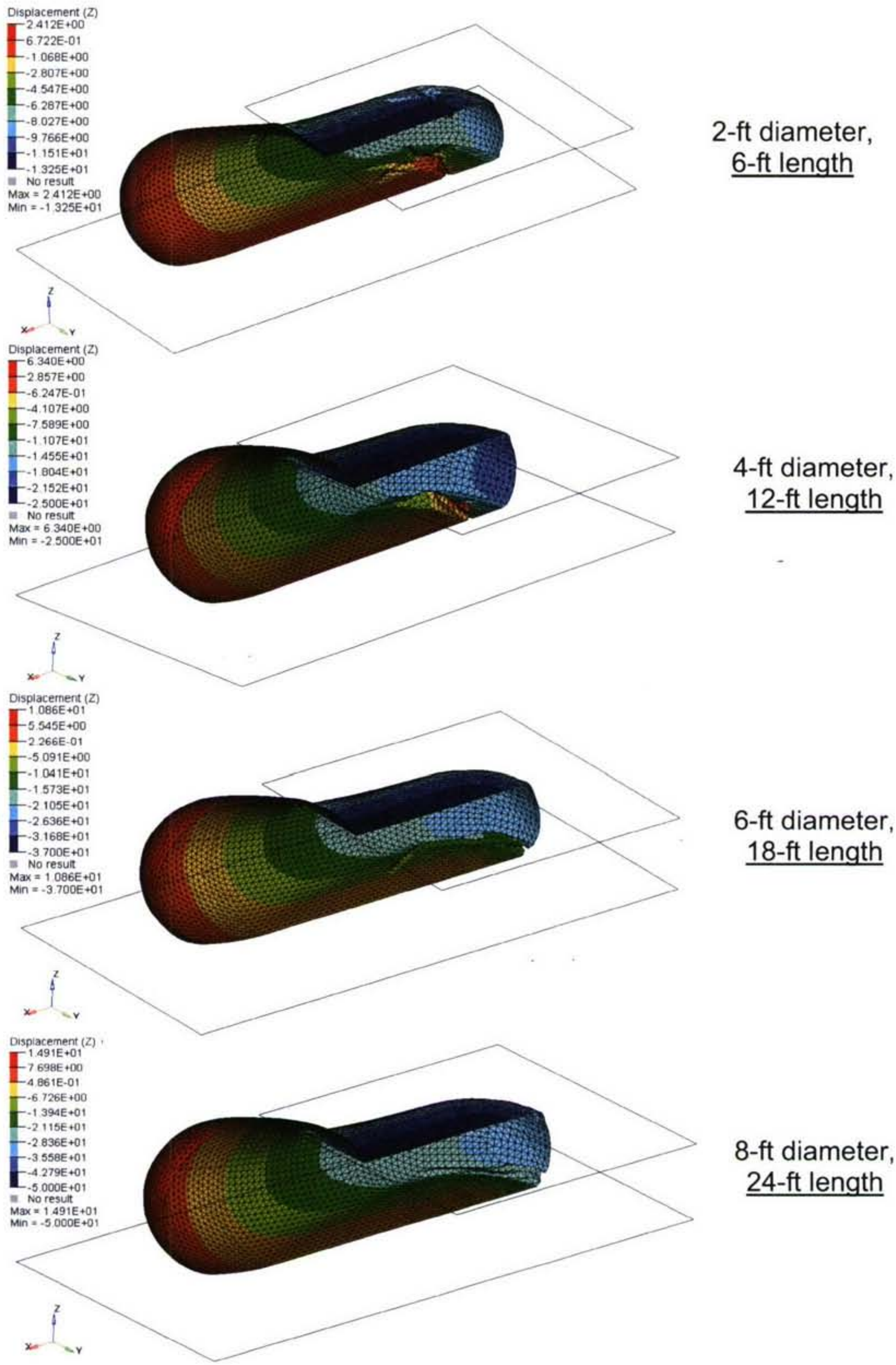

Figure 7. Displacement Contour Plots of 2-, 4-, 6-, and 8-ft Diameter, Half-Symmetry, Ship-to-Causeway Models at Approximately 50% Diametral Compression and 2.5-psi Inflation Pressure

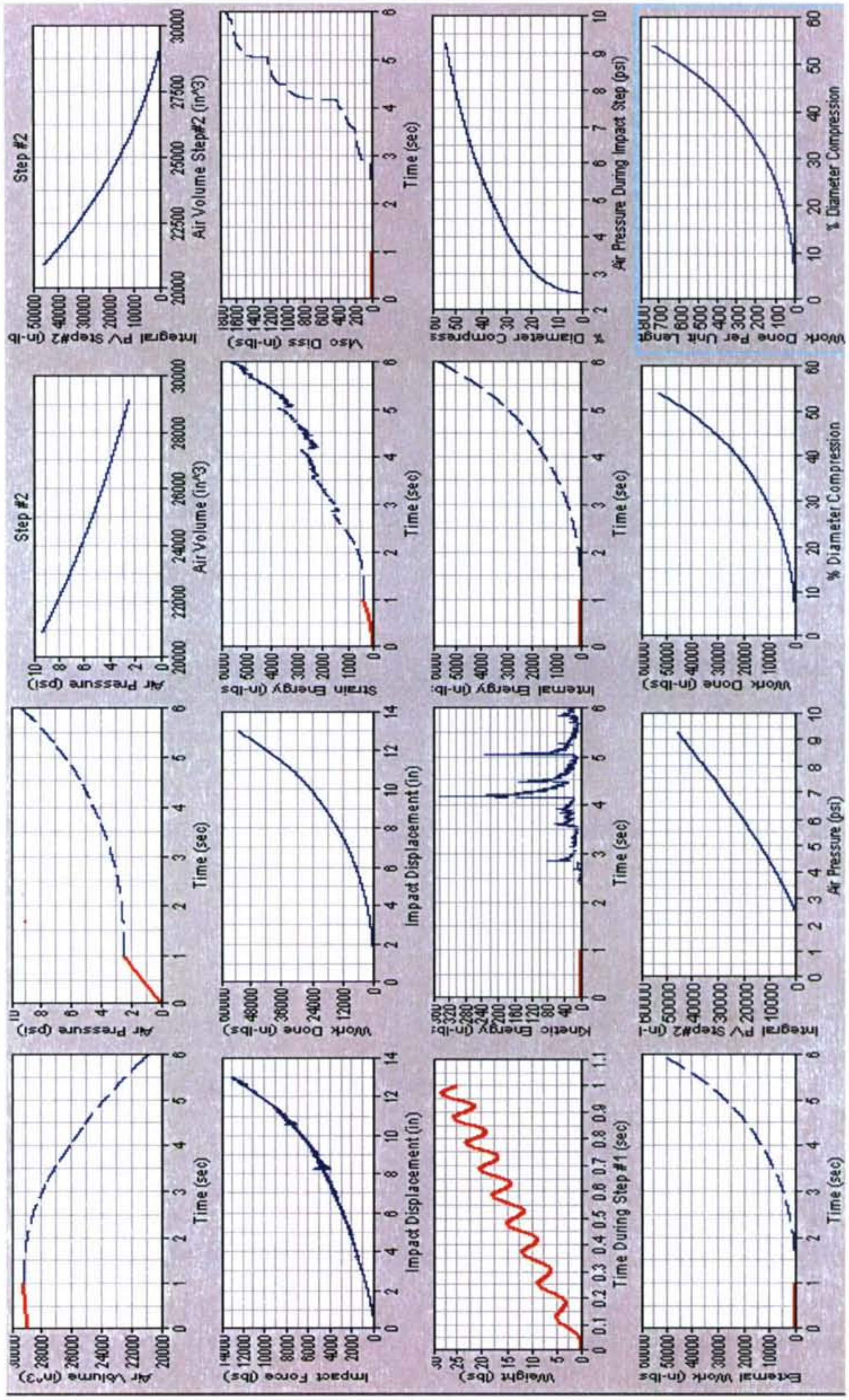

Figure 8. Tracking Results of the 2-ft-Diameter, 6-ft-Long, Ship-to-Ship Model with 2.5-psi Inflation Pressure

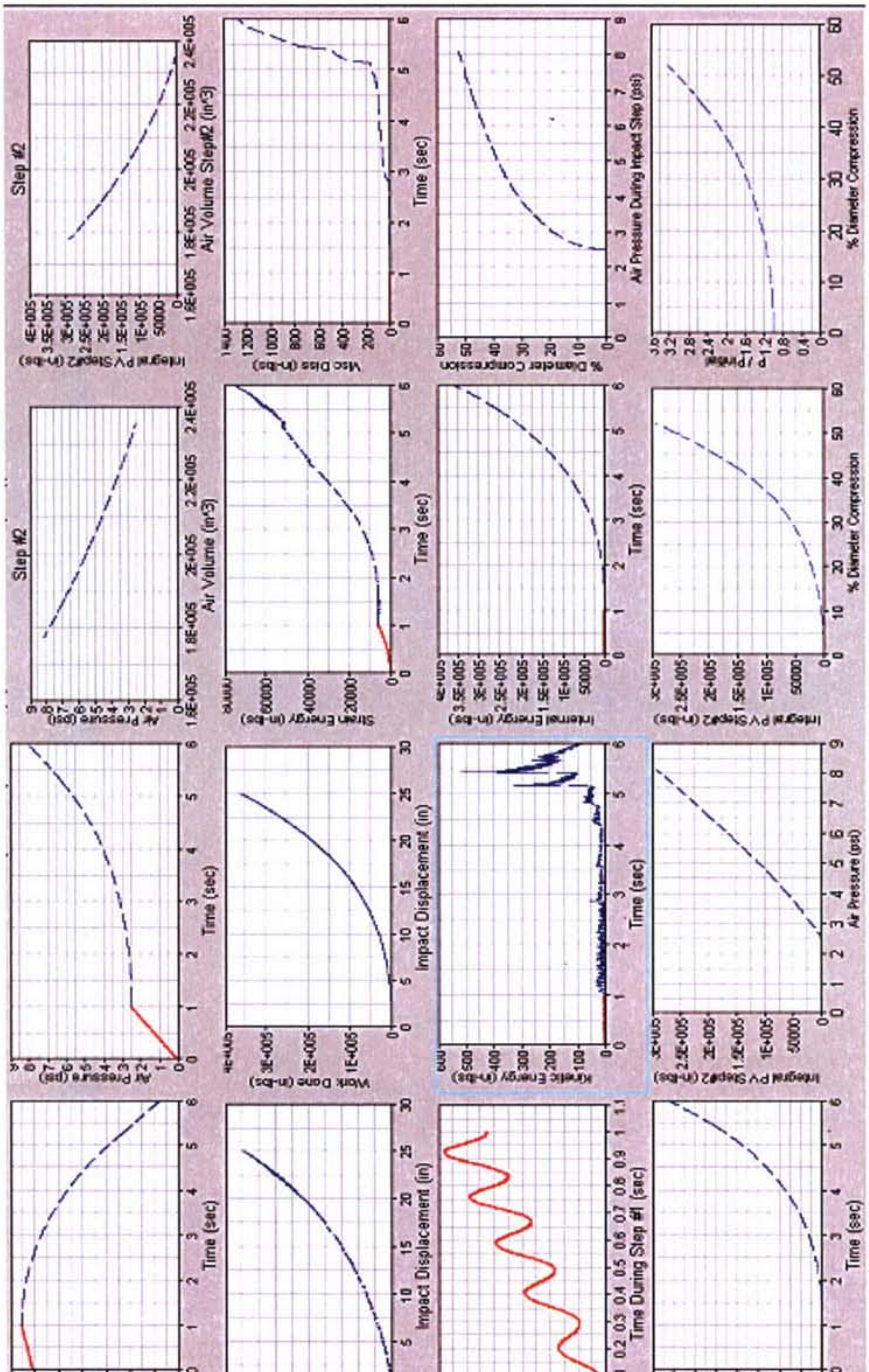

Figure 9. Tracking Results of the 4-ft-Diameter, 12-ft-Long, Ship-to-Ship Model with 2.5-psi Inflation Pressure

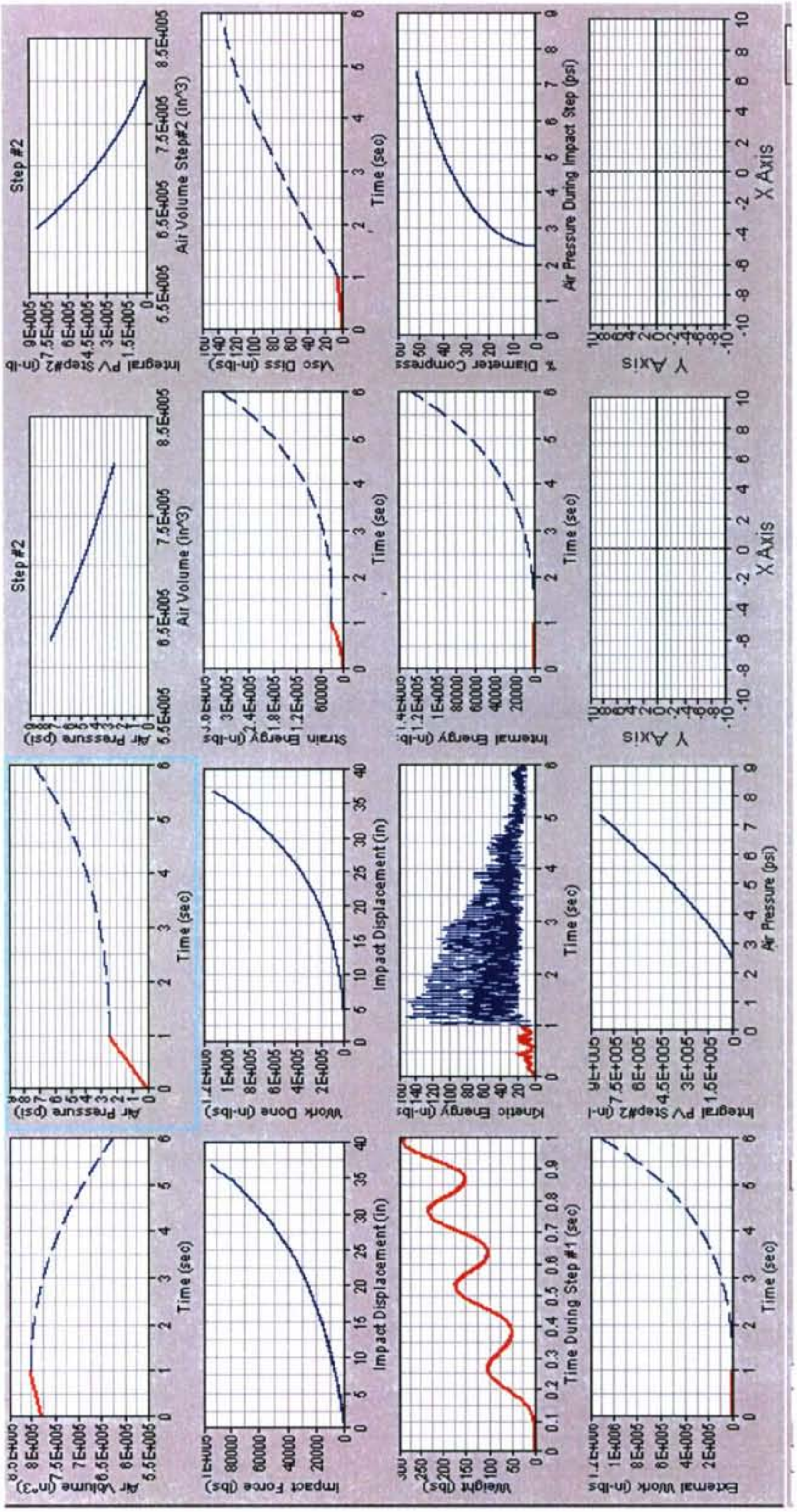

Figure 10. Tracking Results of the 6-ft-Diameter, 18-ft-Long, Ship-to-Ship Model with 2.5-psi Inflation Pressure

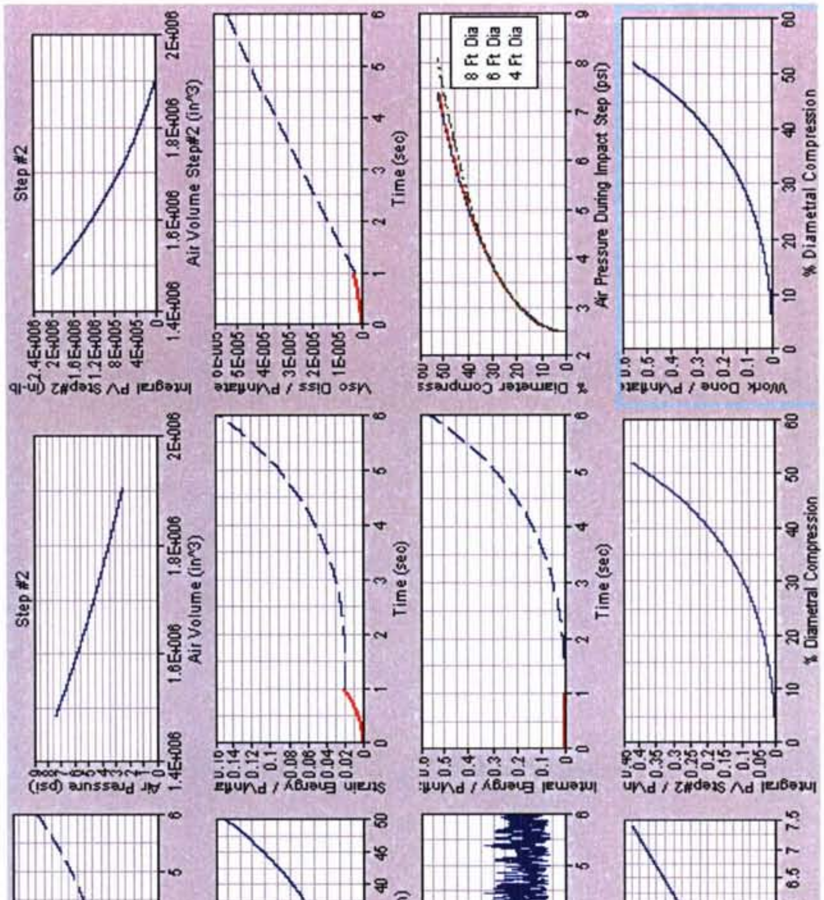

Figure 11. Tracking Results of the 8-ft-Diameter, 24-ft-Long, Ship-to-Ship Model with 2.5-psi Inflation Pressure

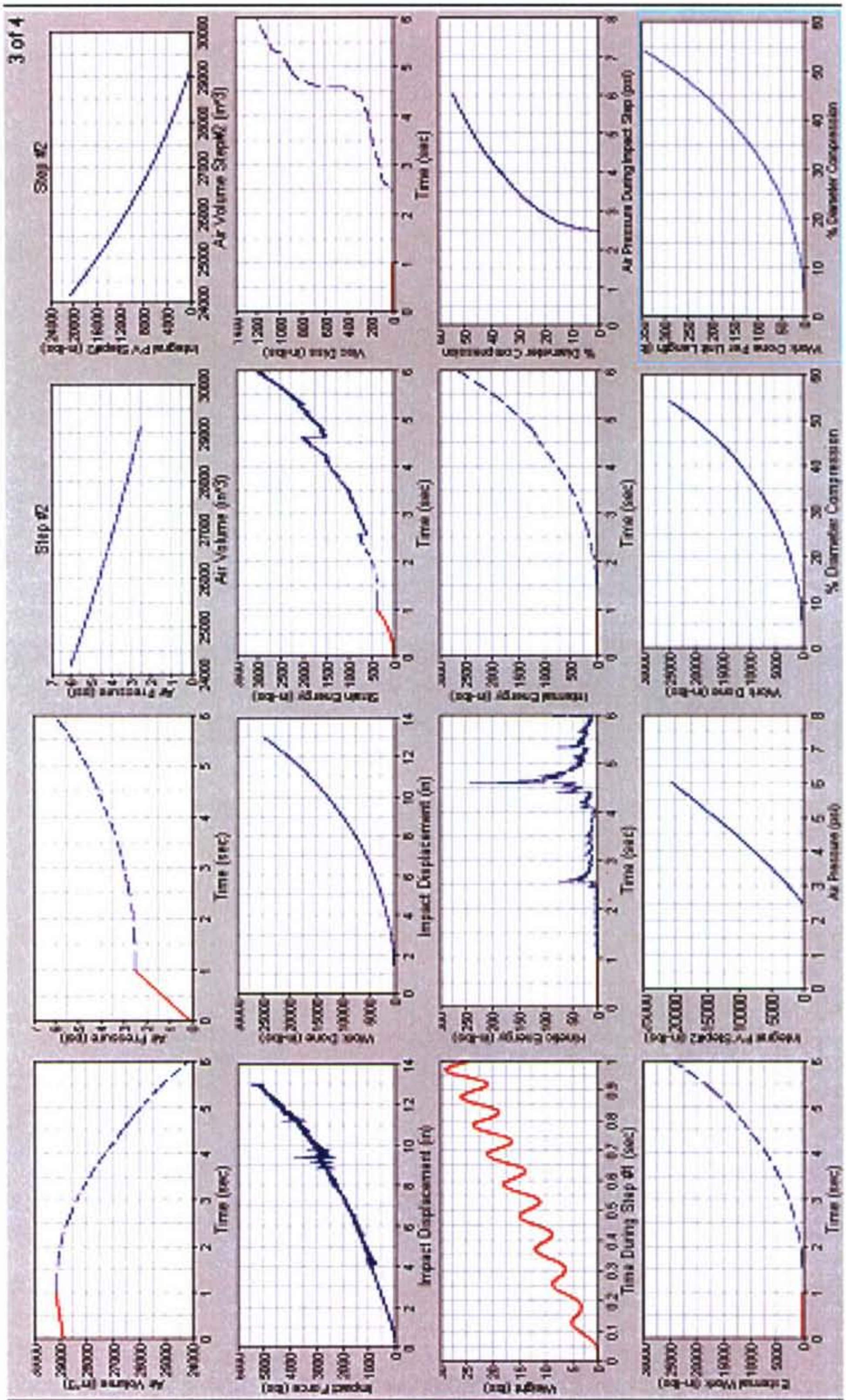

Figure 12. Tracking Results of the 2-ft-Diameter, 6-ft-Long, Ship-to-Causeway Model with 2.5-psi Inflation Pressure

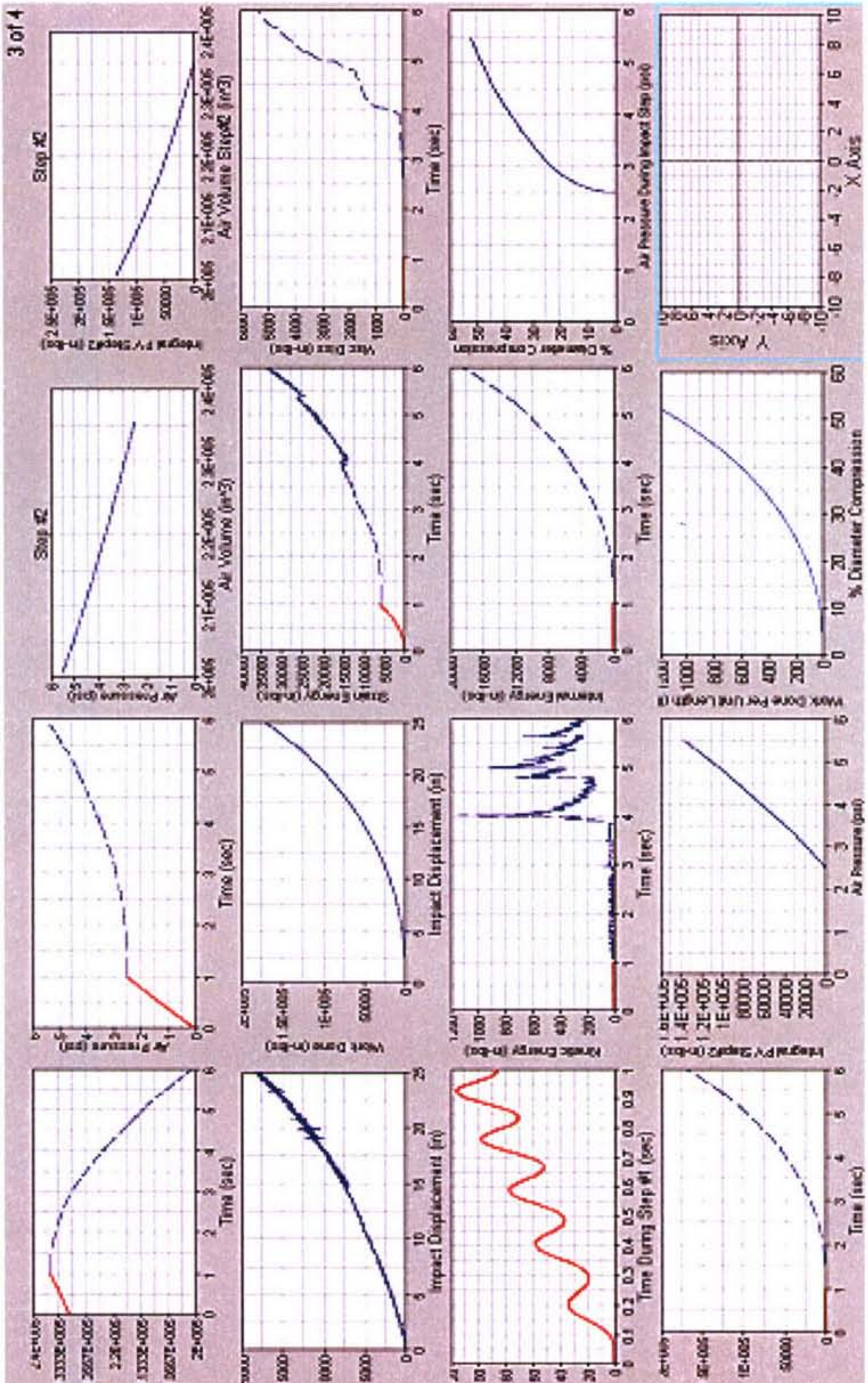

Figure 13. Tracking Results of the 4-ft-Diameter, 12-ft-Long, Ship-to-Causeway Model with 2.5-psi Inflation Pressure

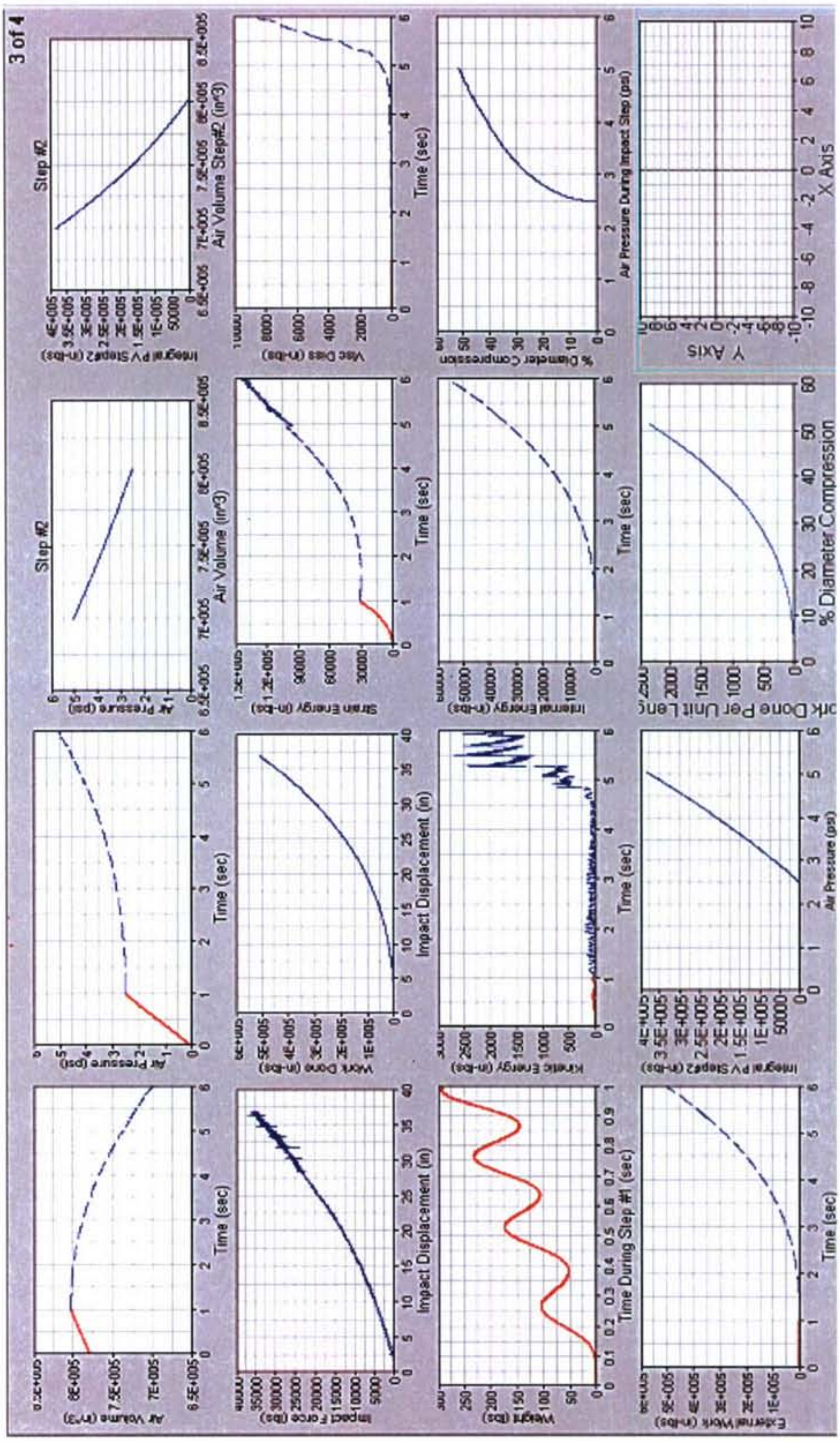

Figure 14. Tracking Results of the 6-ft-Diameter, 18-ft-Long, Ship-to-Causeway Model with 2.5-psi Inflation Pressure

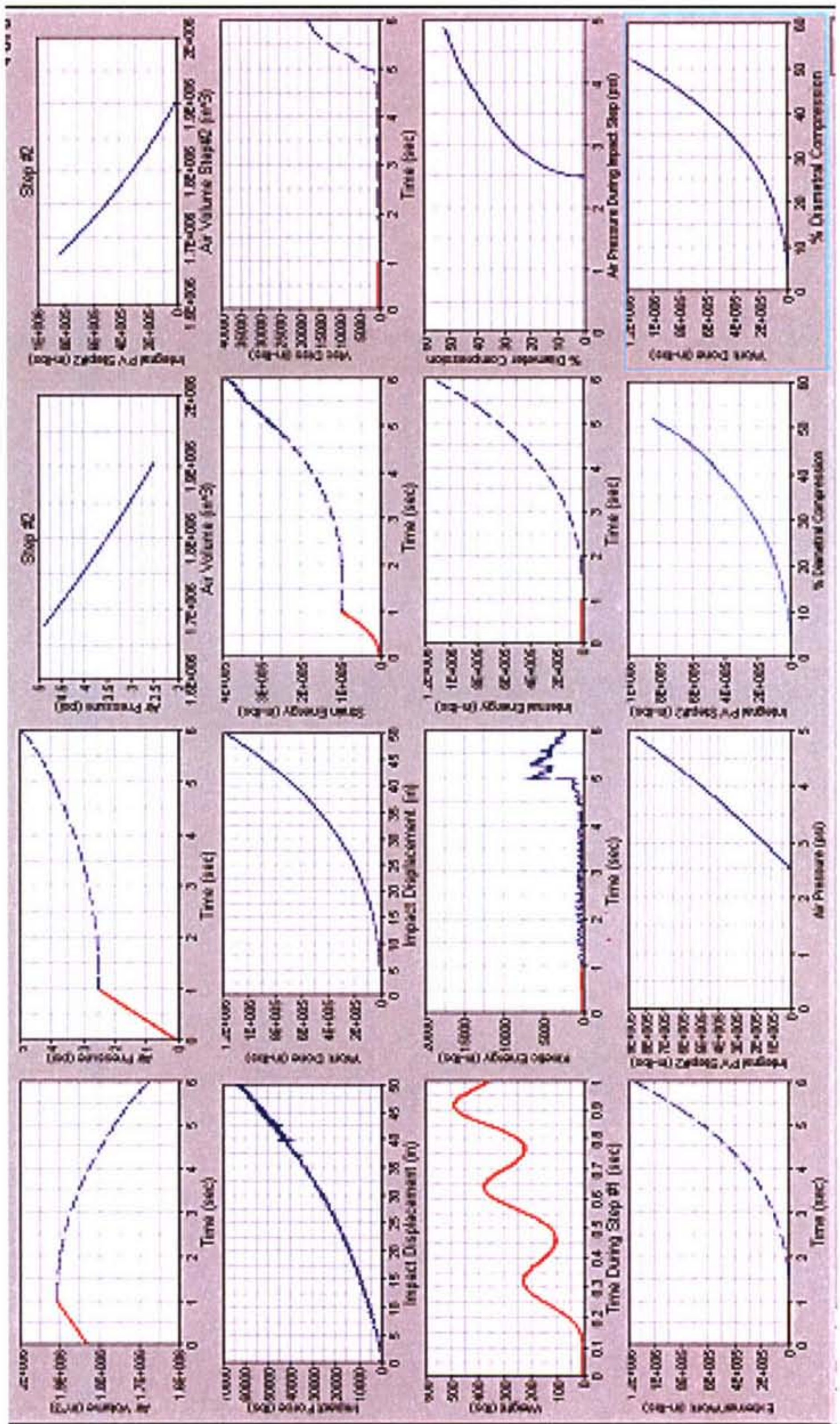

Figure 15. Tracking Results of the 8-ft-Diameter, 24-ft-Long, Ship-to-Causeway Model with 2.5-psi Inflation Pressure

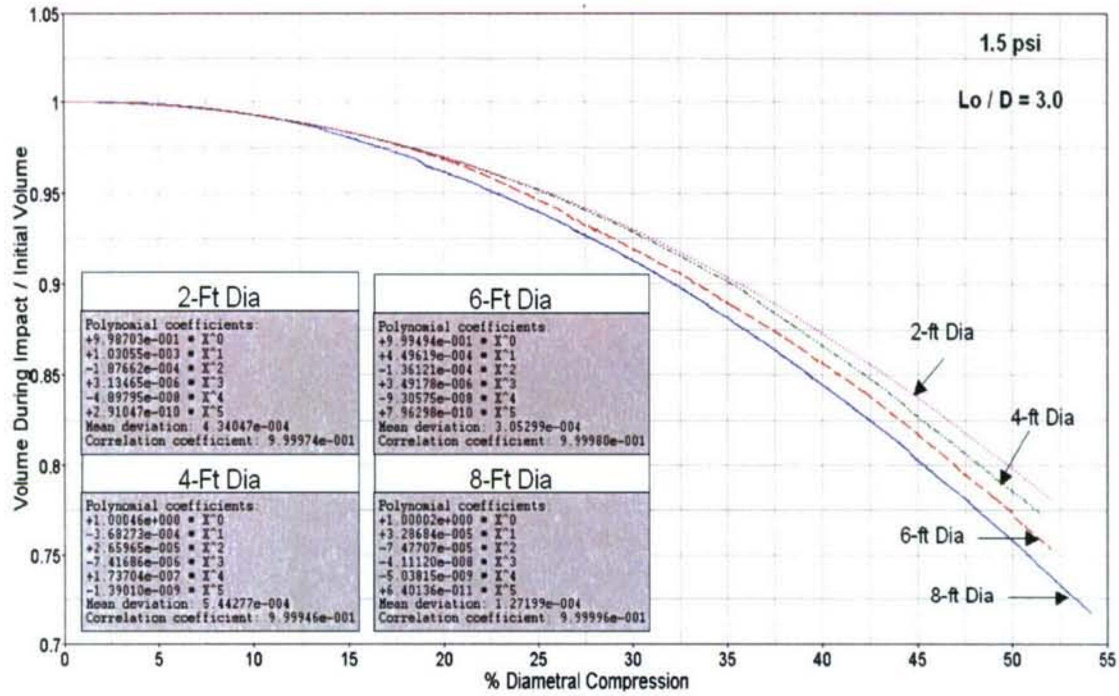

Figure 16. Normalized Volume Versus Percent Diametral Compression Curves for Ship-to-Ship Models at 1.5-psi Inflation Pressure

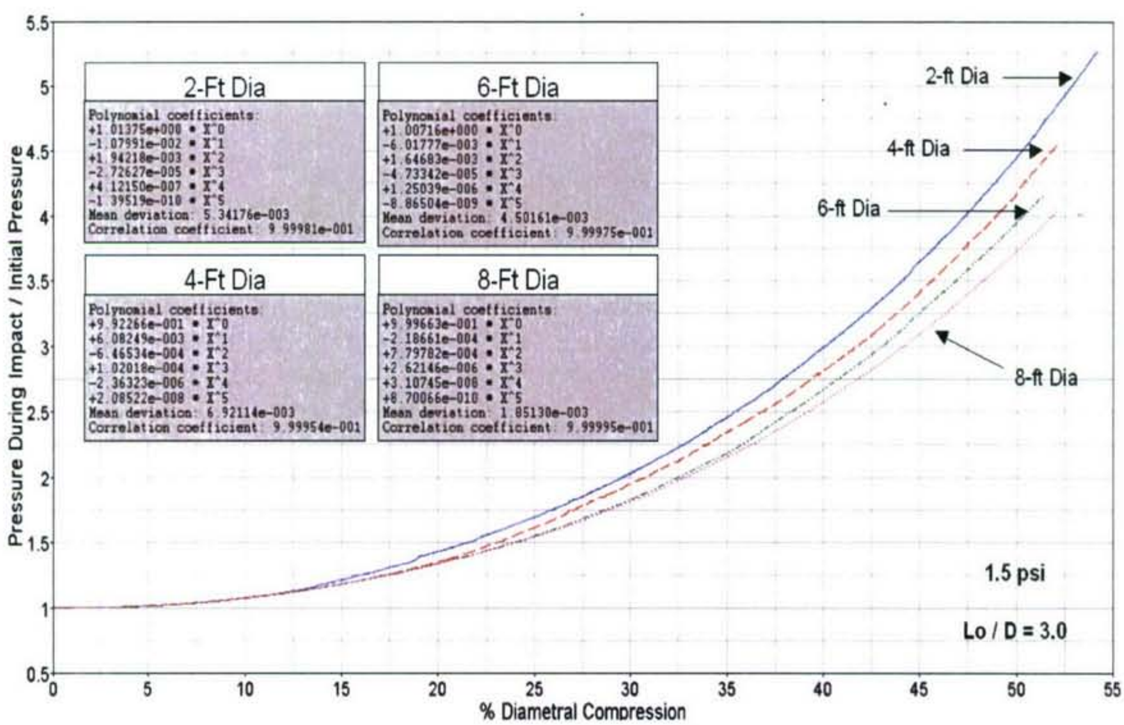

Figure 17. Normalized Pressure Versus Percent Diametral Compression Curves for Ship-to-Ship Models at 1.5-psi Inflation Pressure

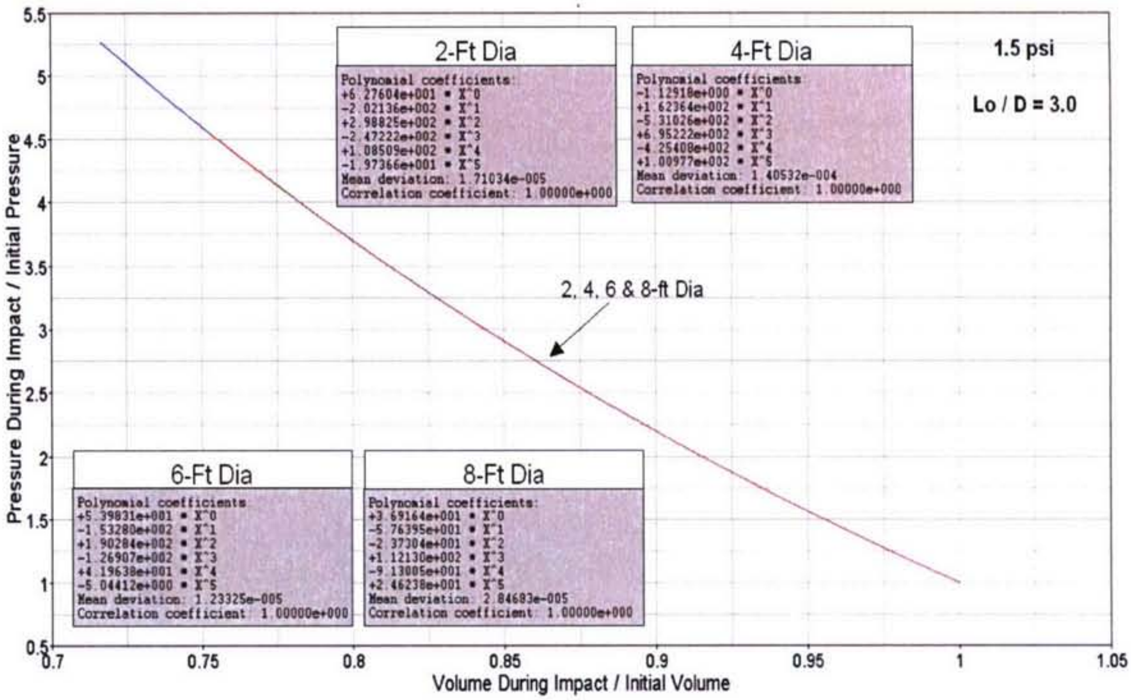

Figure 18. Normalized Pressure Versus Volume Curves for Ship-to-Ship Models at 1.5-psi Inflation Pressure

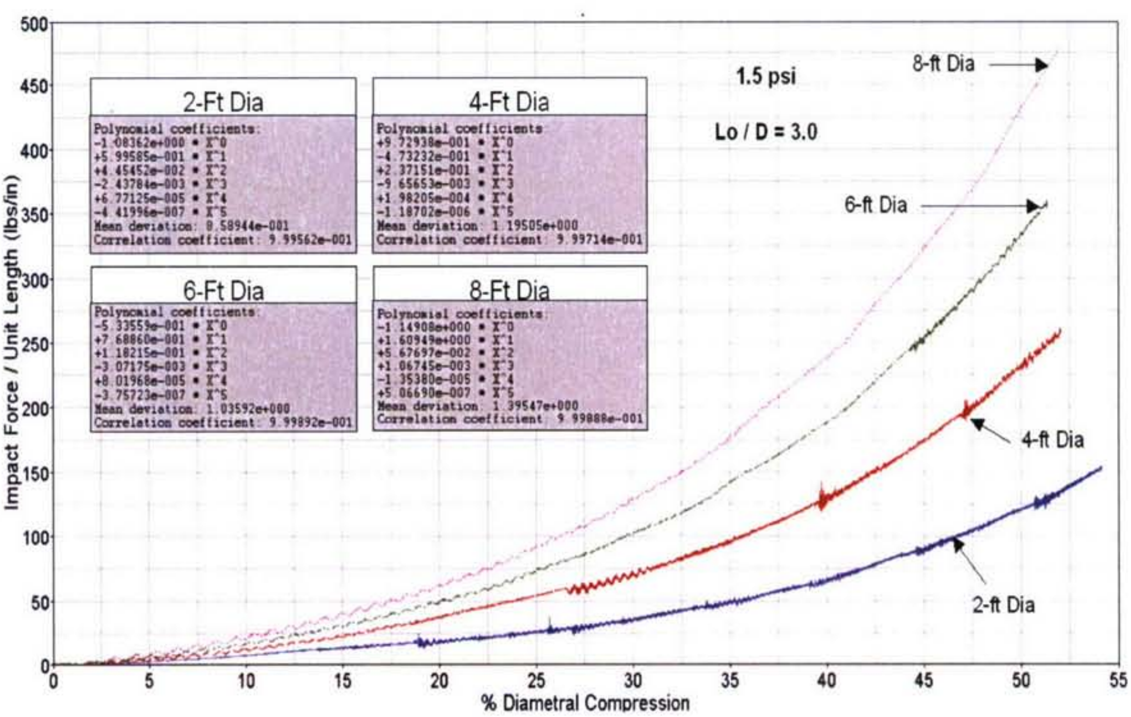

Figure 19. Impact Force per Unit Fender Length Versus Percent Diametral Compression Curves for Ship-to-Ship Models at 1.5-psi Inflation Pressure

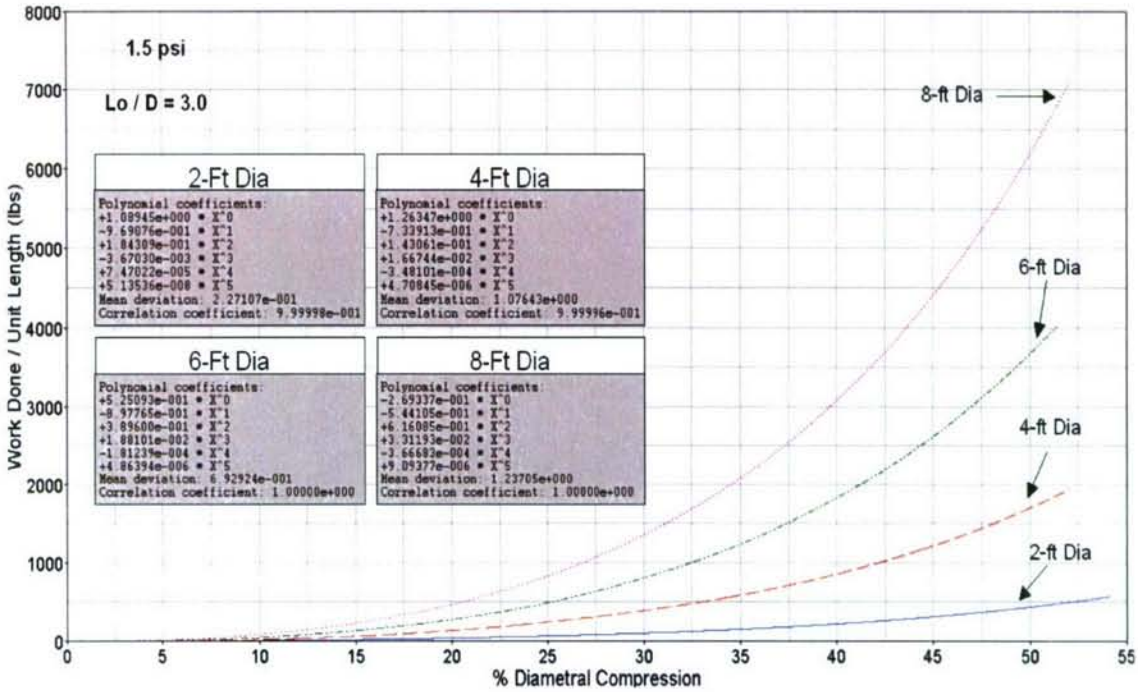

Figure 20. Work Done per Unit Fender Length Versus Percent Diametral Compression Curves for Ship-to-Ship Models at 1.5-psi Inflation Pressure

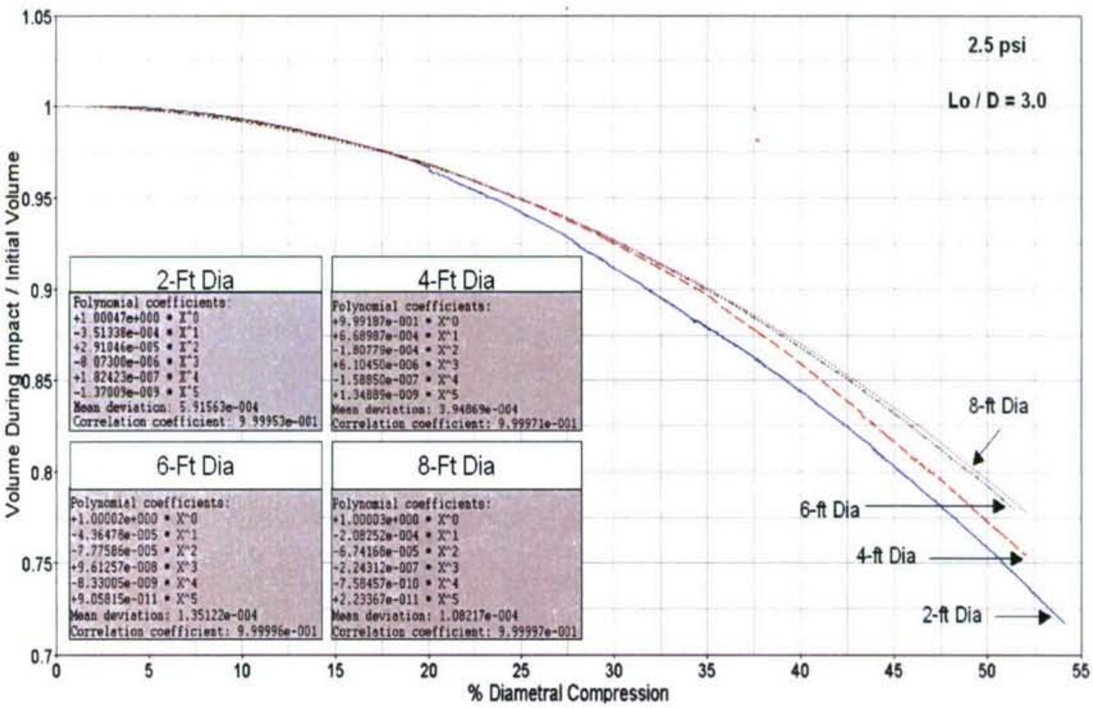

Figure 21. Normalized Volume Versus Percent Diametral Compression Curves for Ship-to-Ship Models at 2.5-psi Inflation Pressure

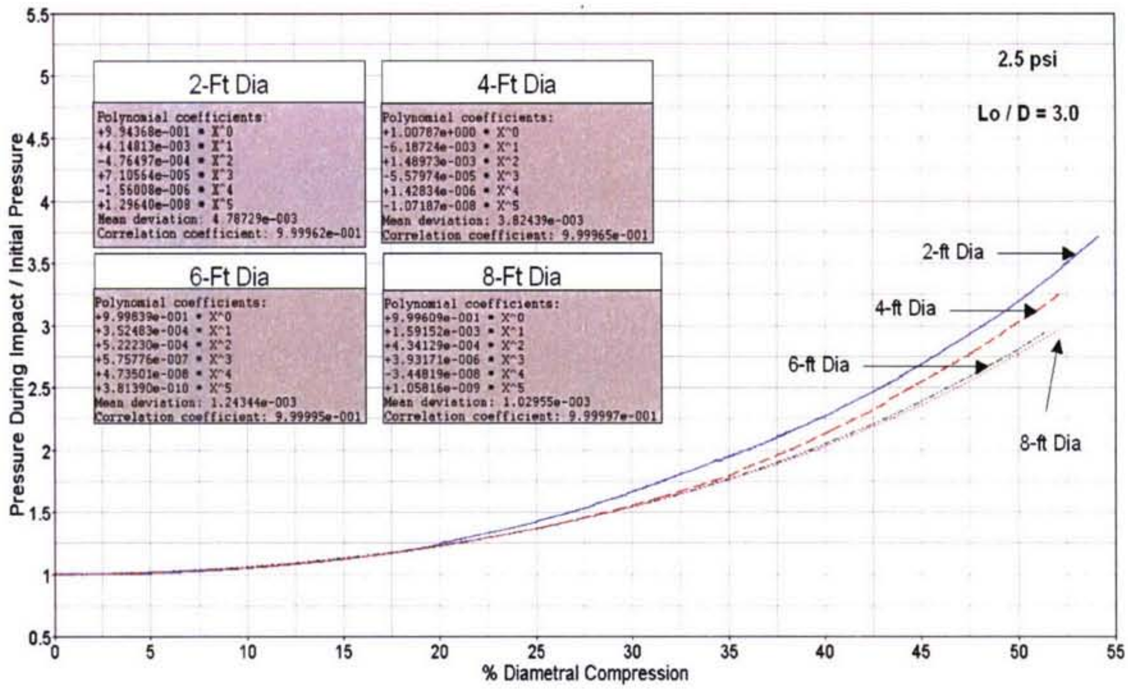

Figure 22. Normalized Pressure Versus Percent Diametral Compression Curves for Ship-to-Ship Models at 2.5-psi Inflation Pressure

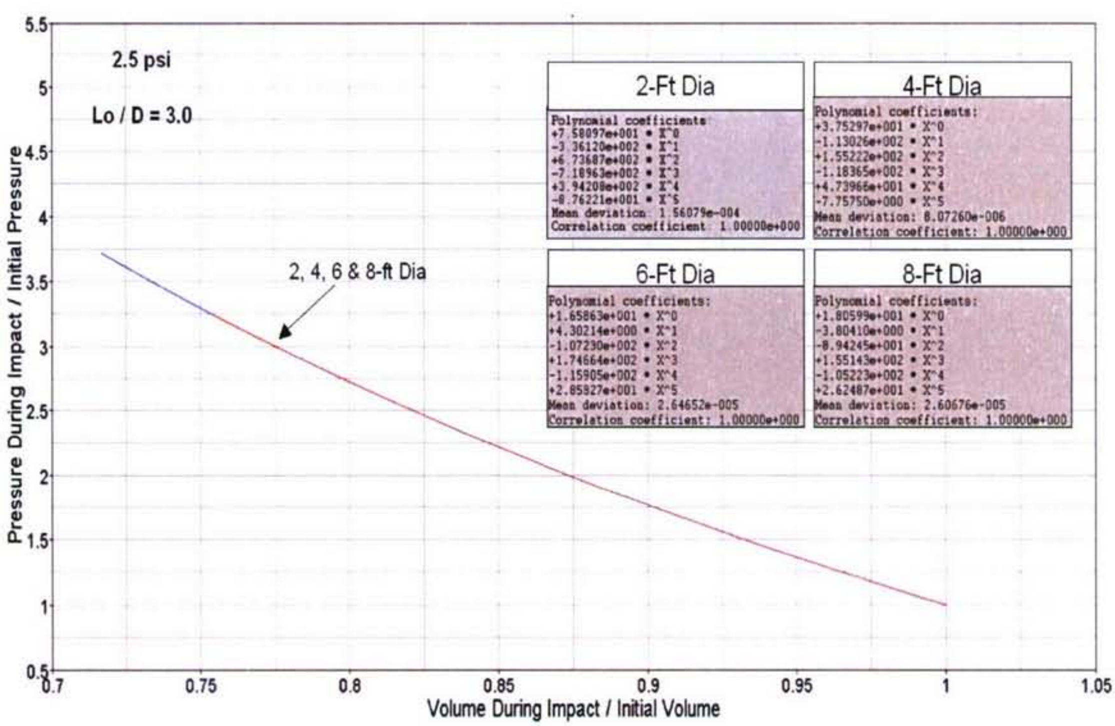

Figure 23. Normalized Pressure Versus Volume Curves for Ship-to-Ship Models at 2.5-psi Inflation Pressure

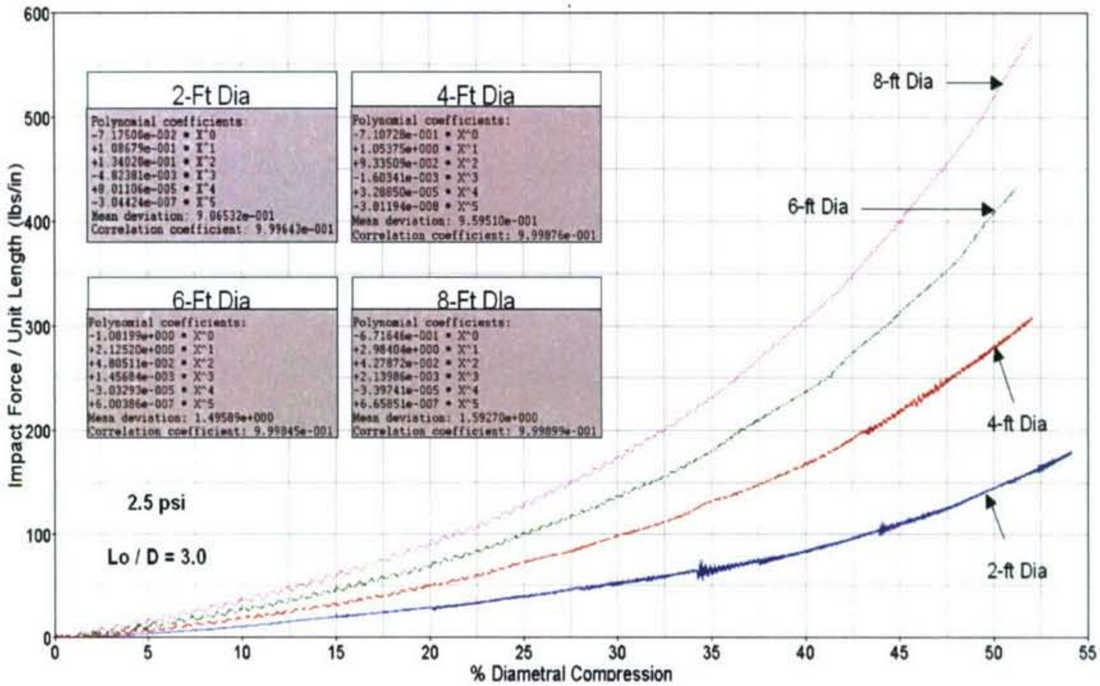

Figure 24. Impact Force per Unit Fender Length Versus Percent Diametral Compression Curves for Ship-to-Ship Models at 2.5-psi Inflation Pressure

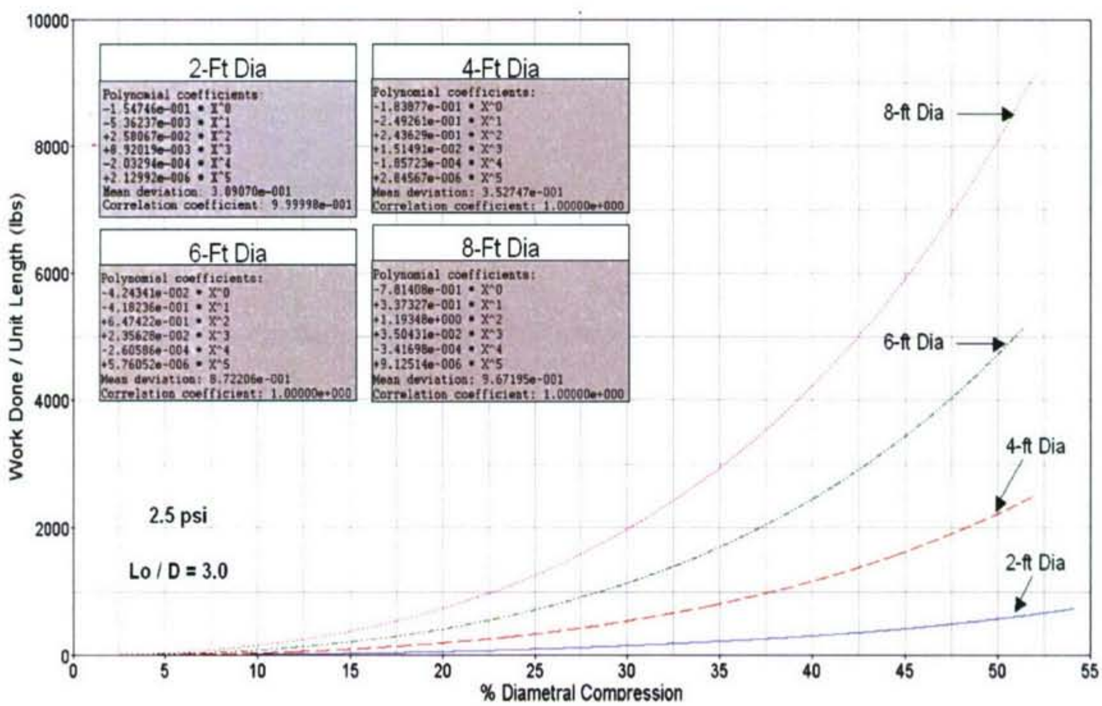

Figure 25. Work Done per Unit Fender Length Versus Percent Diametral Compression Curves for Ship-to-Ship Models at 2.5-psi Inflation Pressure

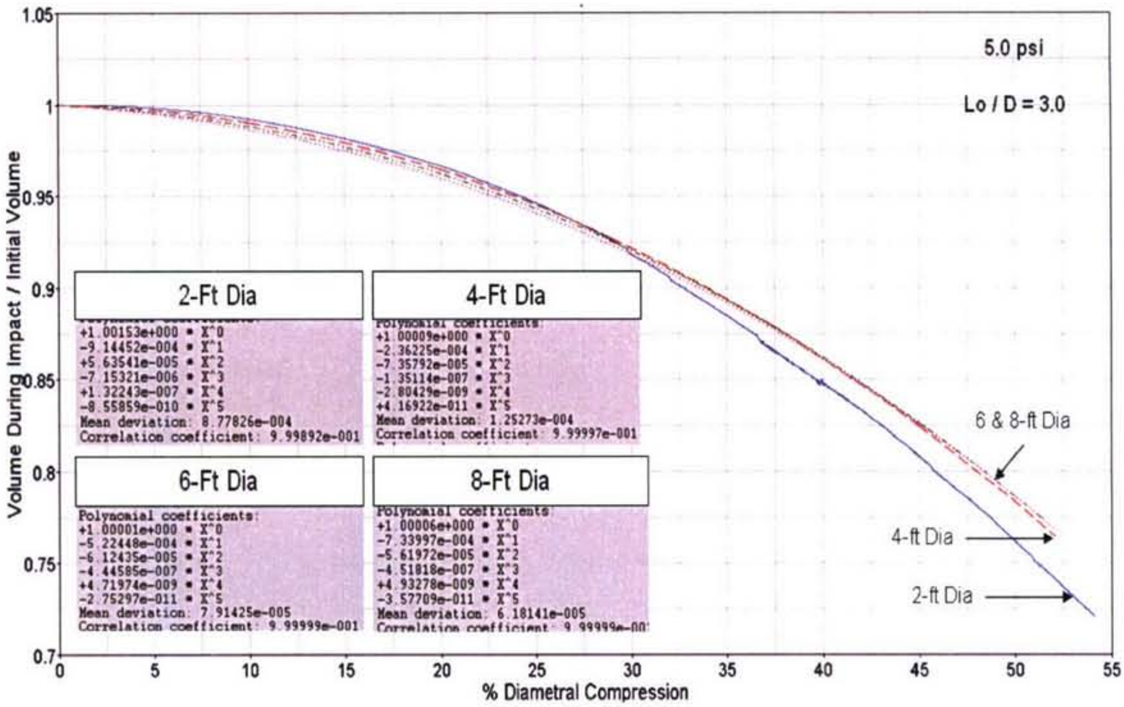

Figure 26. Normalized Volume Versus Percent Diametral Compression Curves for Ship-to-Ship Models at 5.0-psi Inflation Pressure

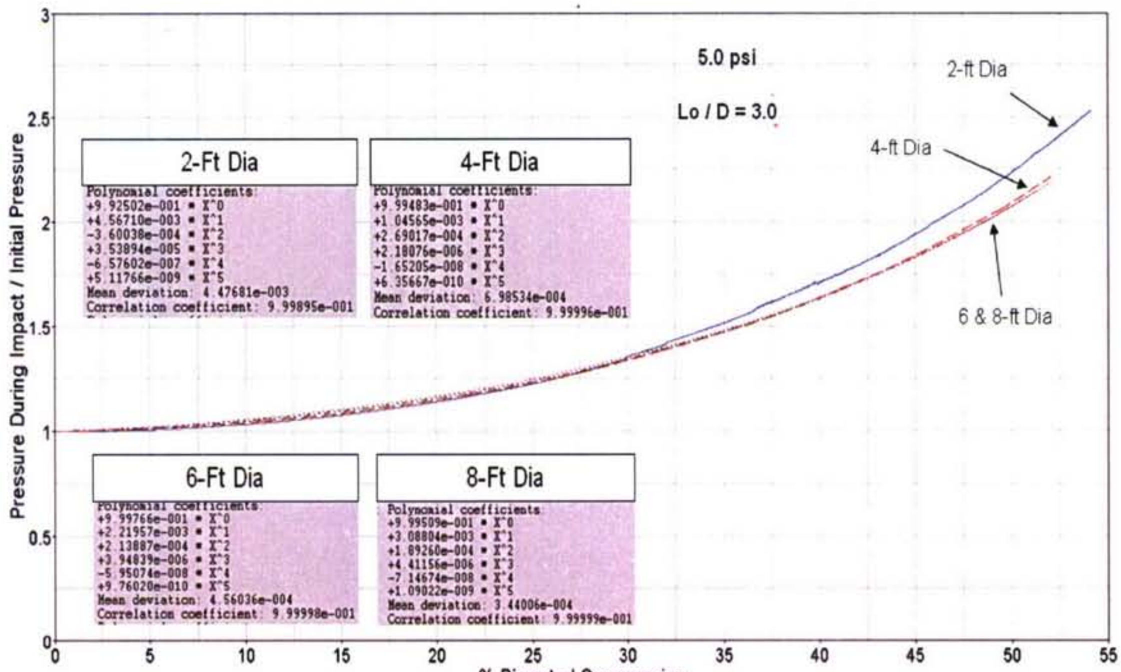

Figure 27. Normalized Pressure Versus Percent Diametral Compression Curves for Ship-to-Ship Models at 5.0-psi Inflation Pressure

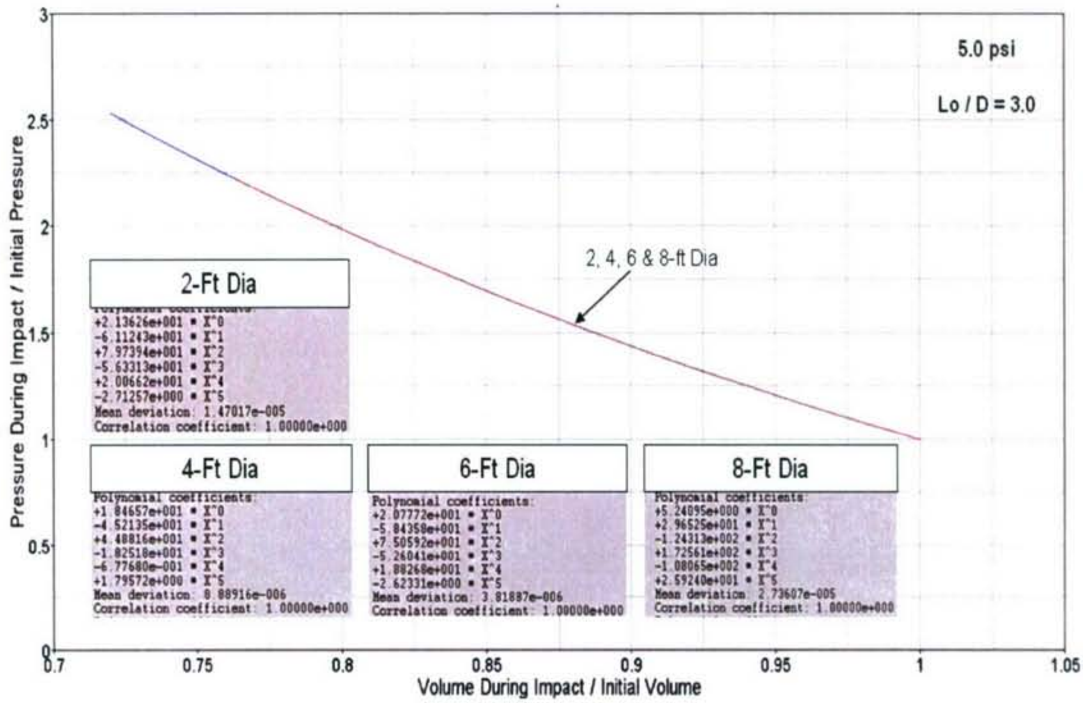

Figure 28. Normalized Pressure Versus Volume Curves for Ship-to-Ship Models at 5.0-psi Inflation Pressure

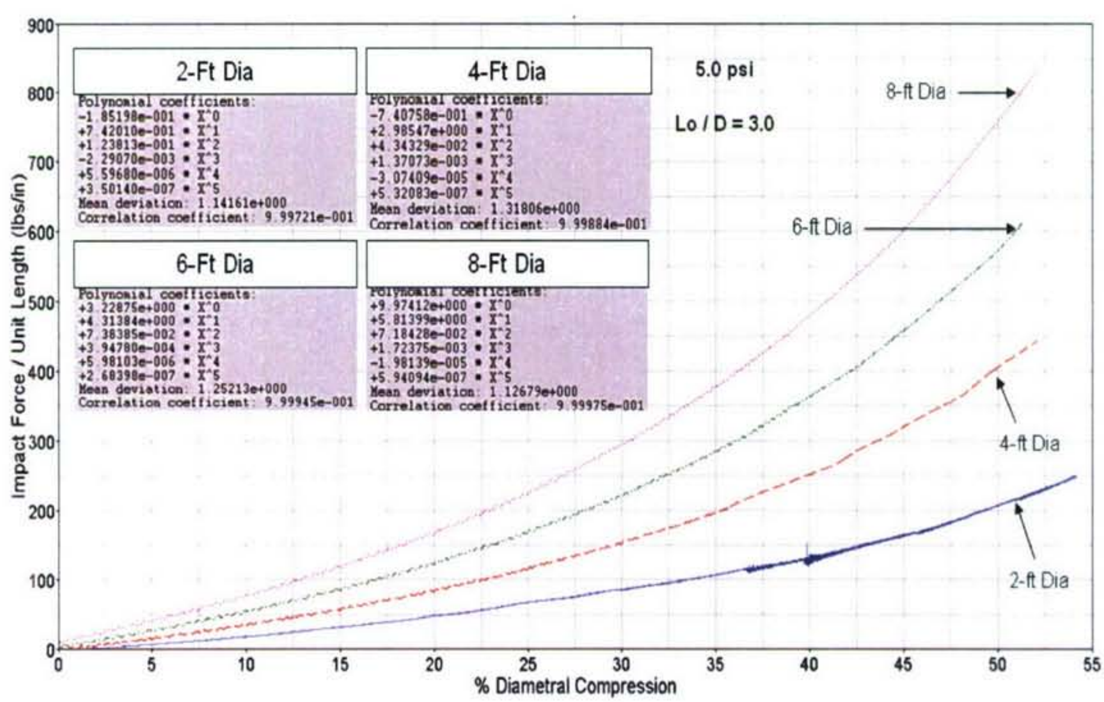

Figure 29. Impact Force per Unit Fender Length Versus Percent Diametral Compression Curves for Ship-to-Ship Models at 5.0-psi Inflation Pressure

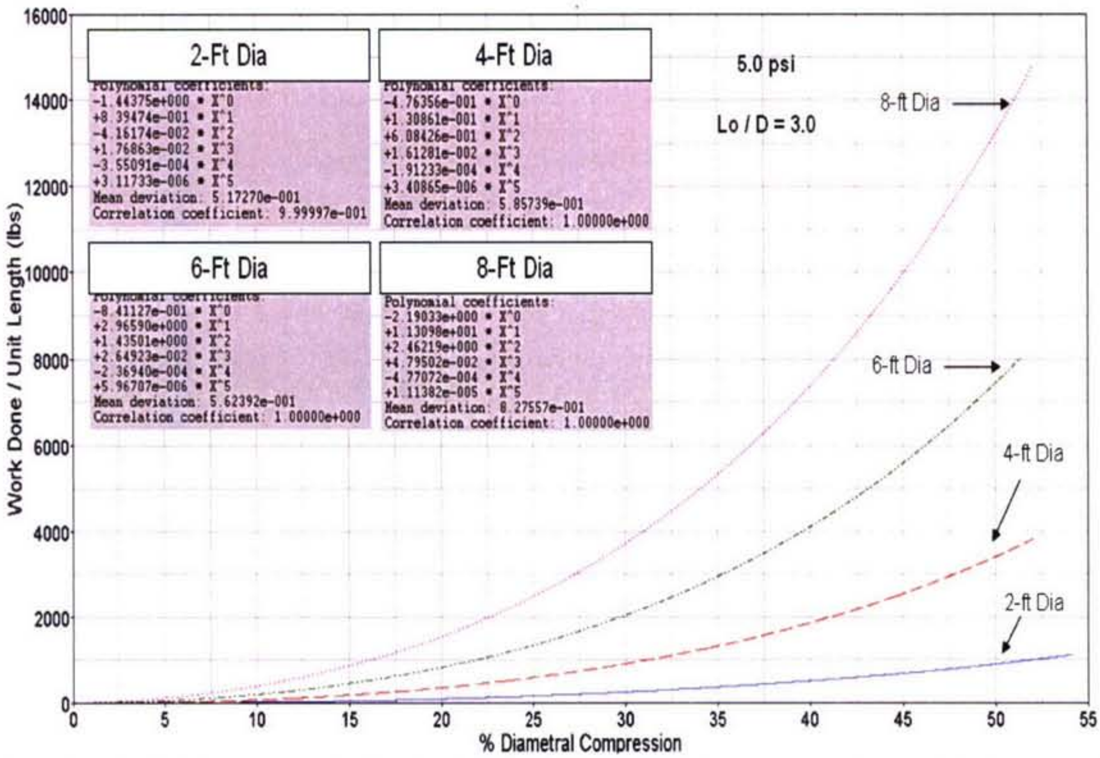

Figure 30. Work Done per Unit Fender Length Versus Percent Diametral Compression Curves for Ship-to-Ship Models at 5.0-psi Inflation Pressure

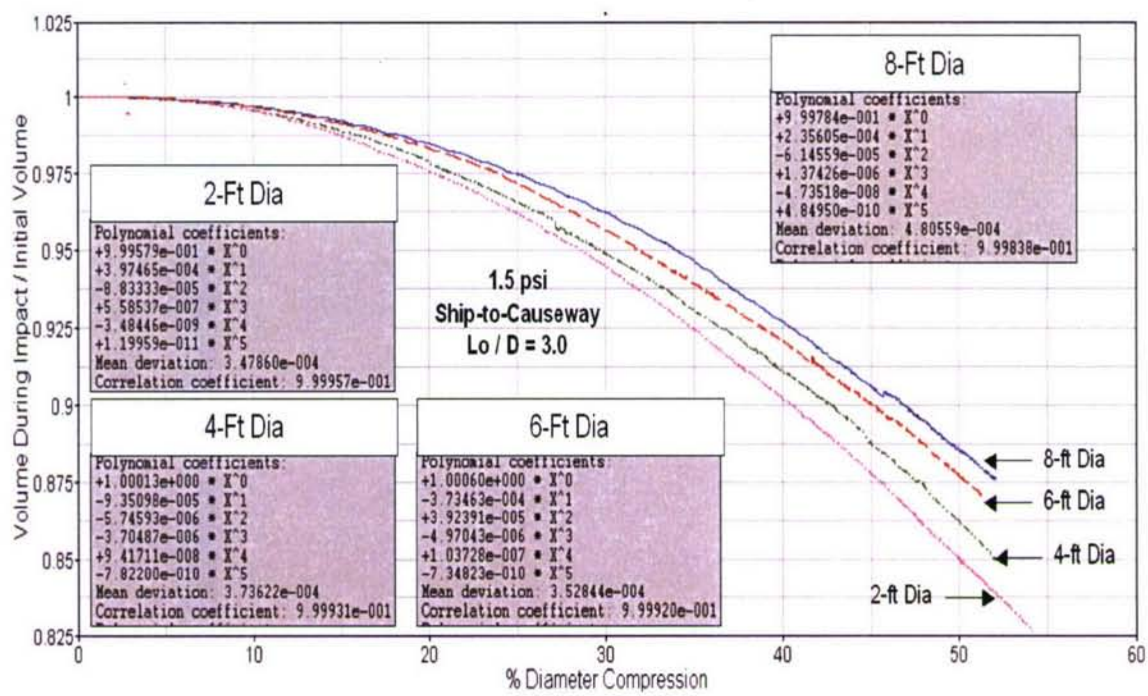

Figure 31. Normalized Volume Versus Percent Diametral Compression Curves for Ship-to-Causeway Models at 1.5-psi Inflation Pressure

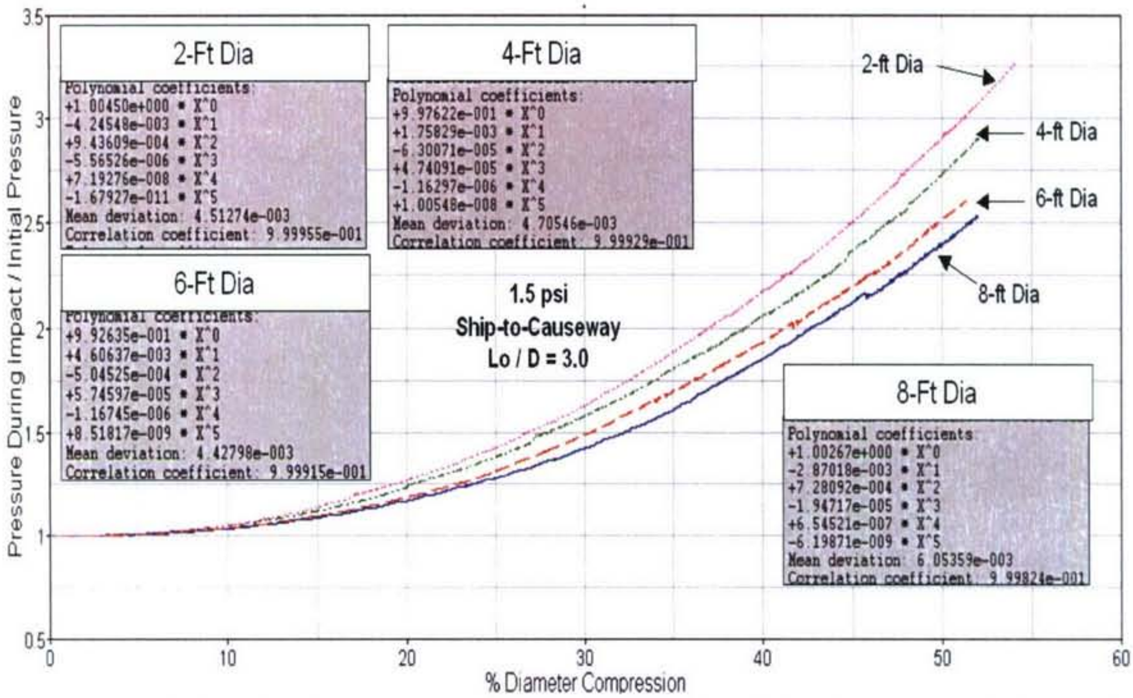

Figure 32. Normalized Pressure Versus Percent Diametral Compression Curves for Ship-to-Causeway Models at 1.5-psi Inflation Pressure

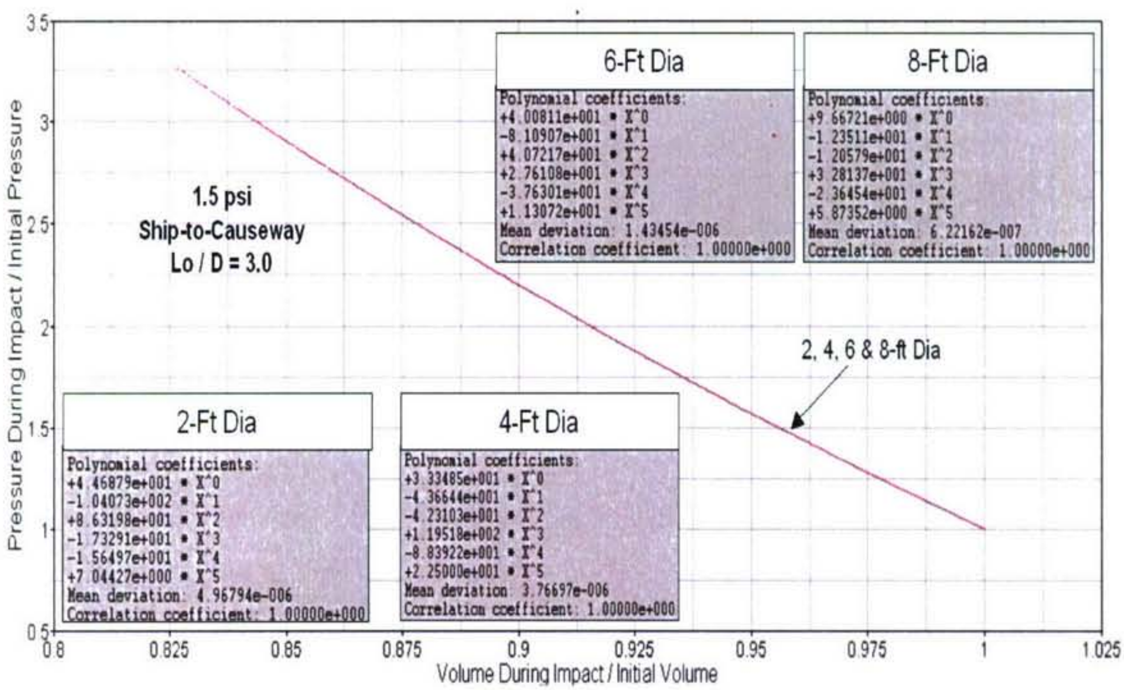

Figure 33. Normalized Pressure Versus Volume Curves for Ship-to-Causeway Models at 1.5-psi Inflation Pressure

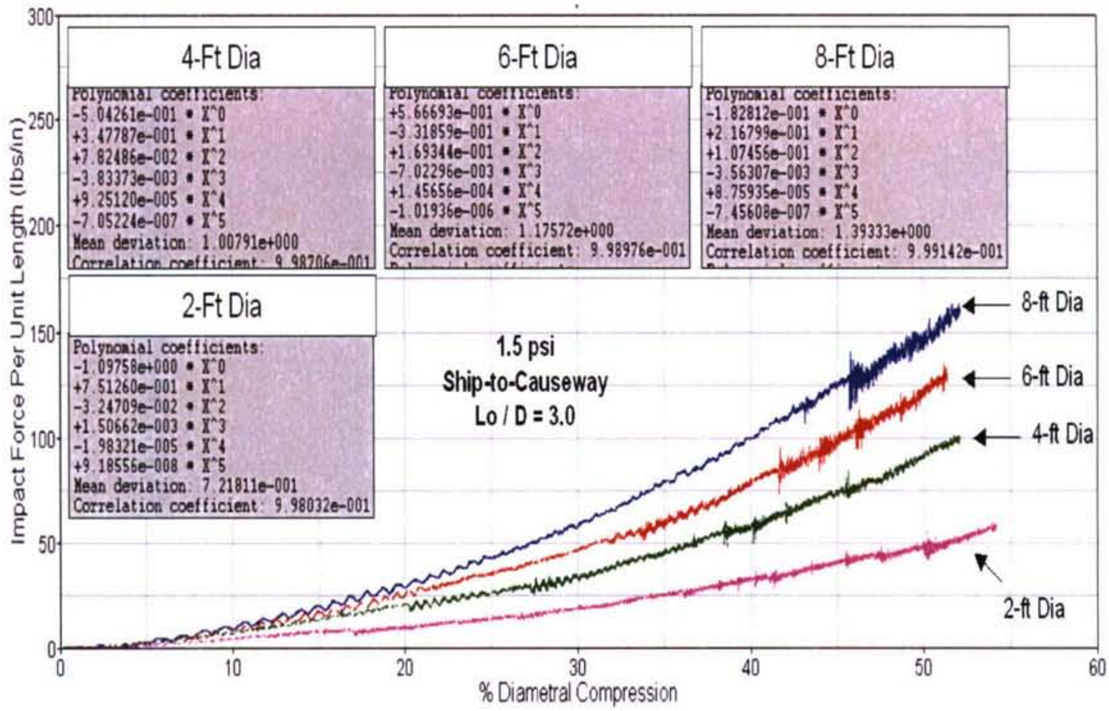

Figure 34. Impact Force per Unit Fender Length Versus Percent Diametral Compression Curves for Ship-to-Causeway Models at 1.5-psi Inflation Pressure

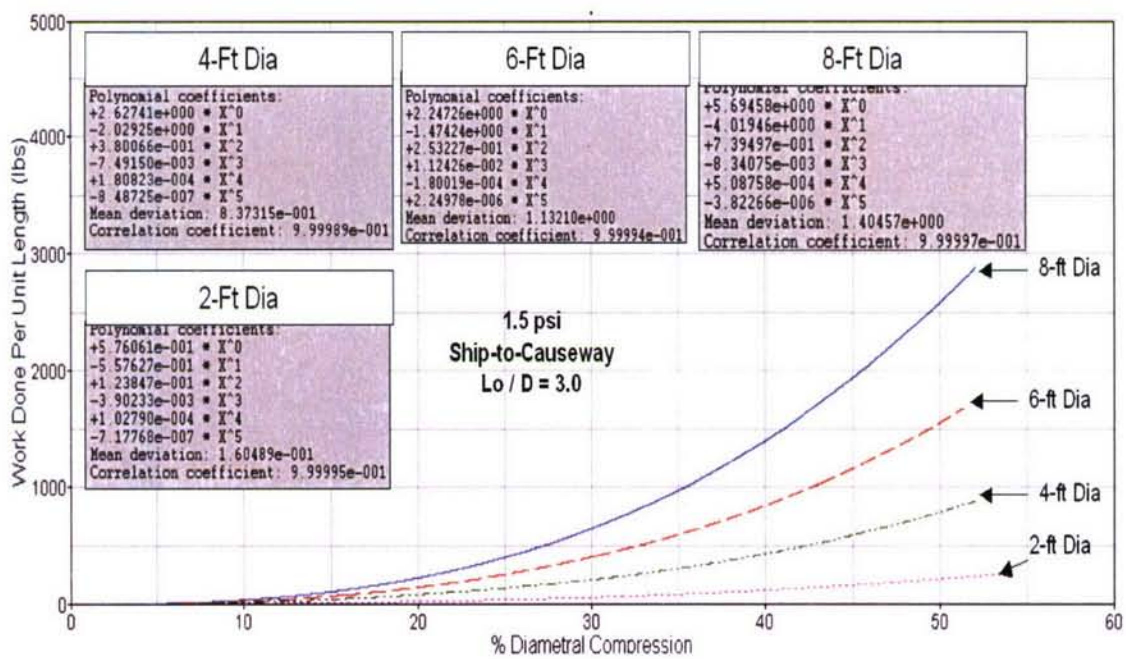

Figure 35. Work Done per Unit Fender Length Versus Percent Diametral Compression Curves for Ship-to-Causeway Models at 1.5-psi Inflation Pressure

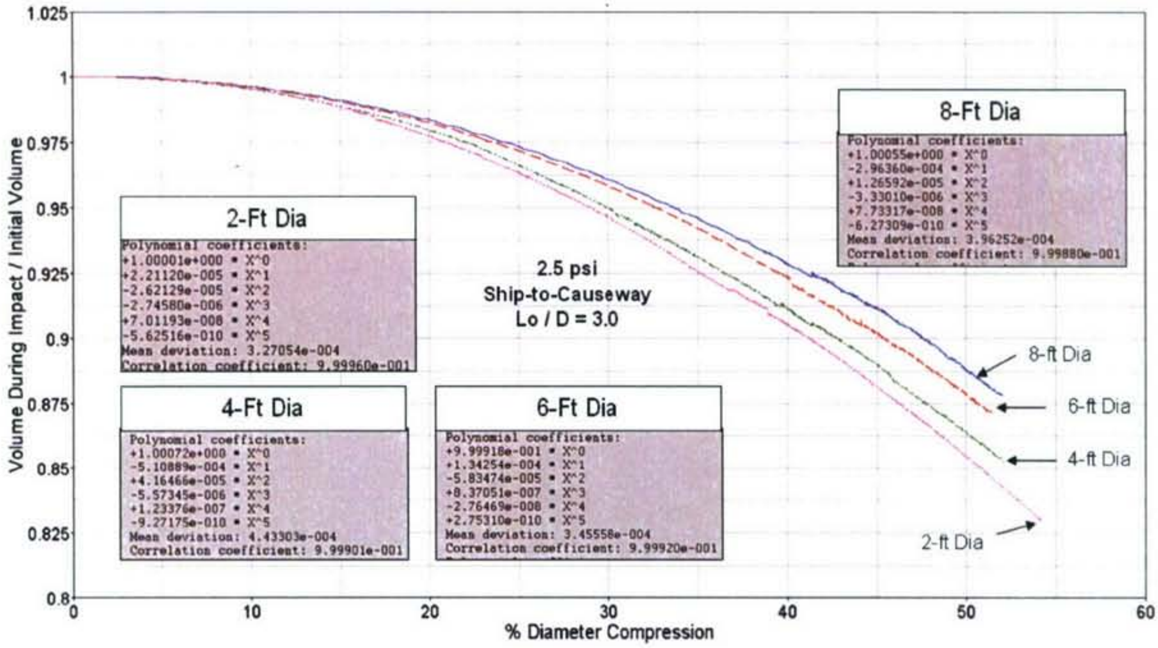

Figure 36. Normalized Volume Versus Percent Diametral Compression Curves for Ship-to-Causeway Models at 2.5-psi Inflation Pressure

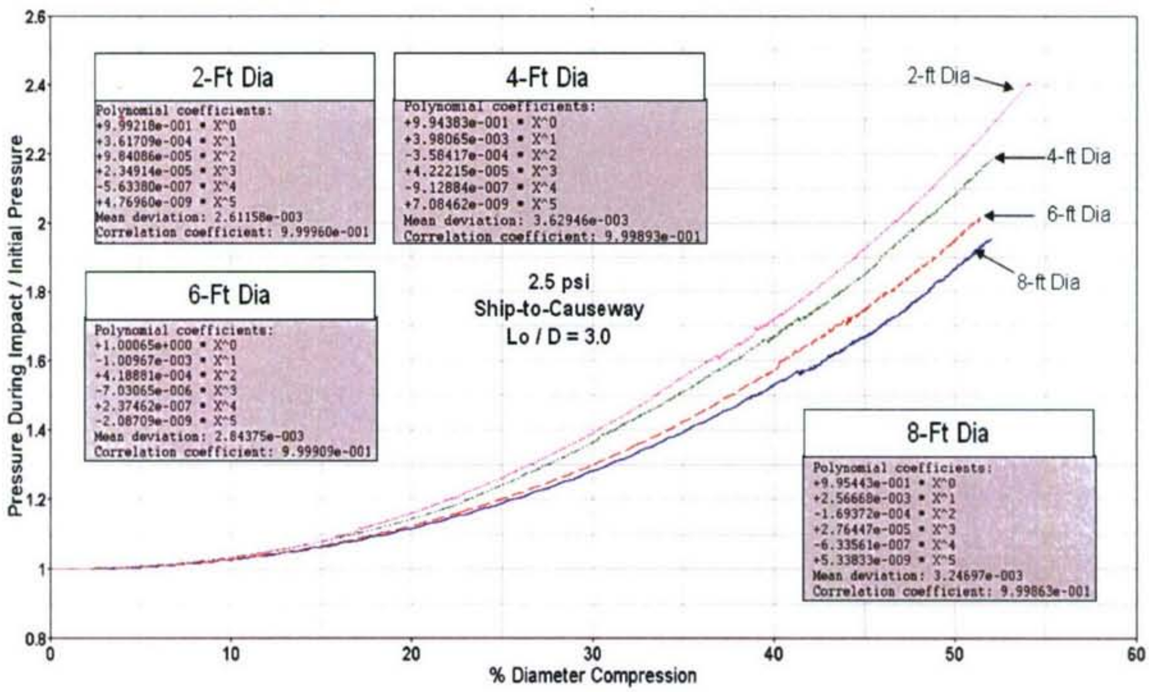

Figure 37. Normalized Pressure Versus Percent Diametral Compression Curves for Ship-to-Causeway Models at 2.5-psi Inflation Pressure

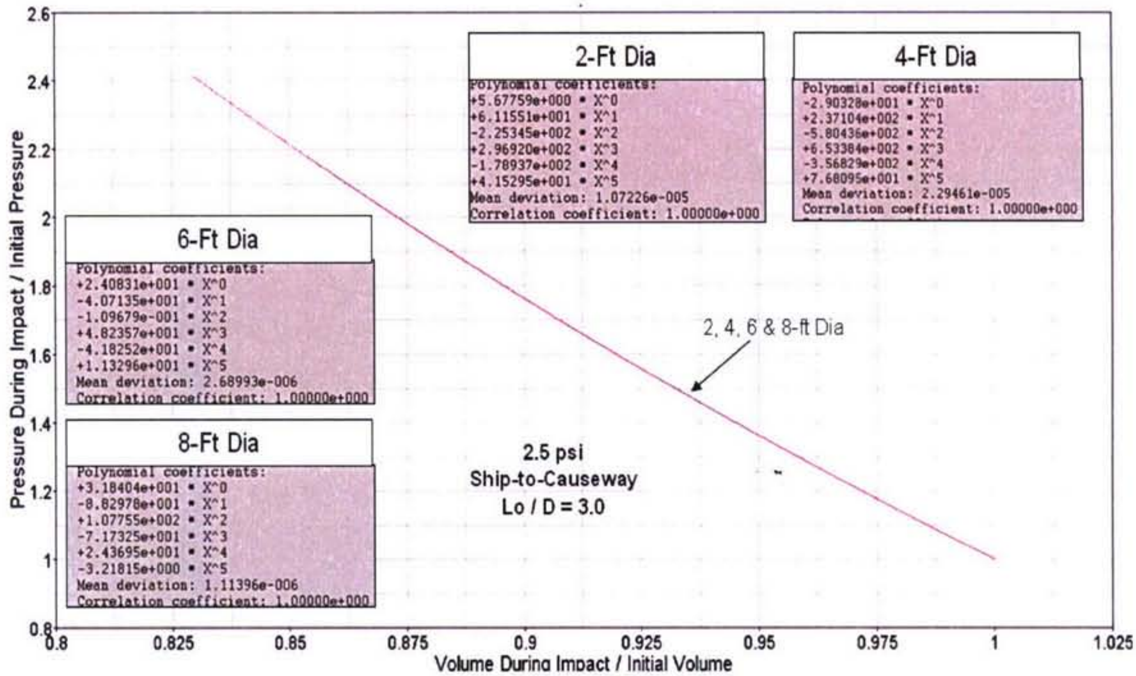

Figure 38. Normalized Pressure Versus Volume Curves for Ship-to-Causeway Models at 2.5-psi Inflation Pressure

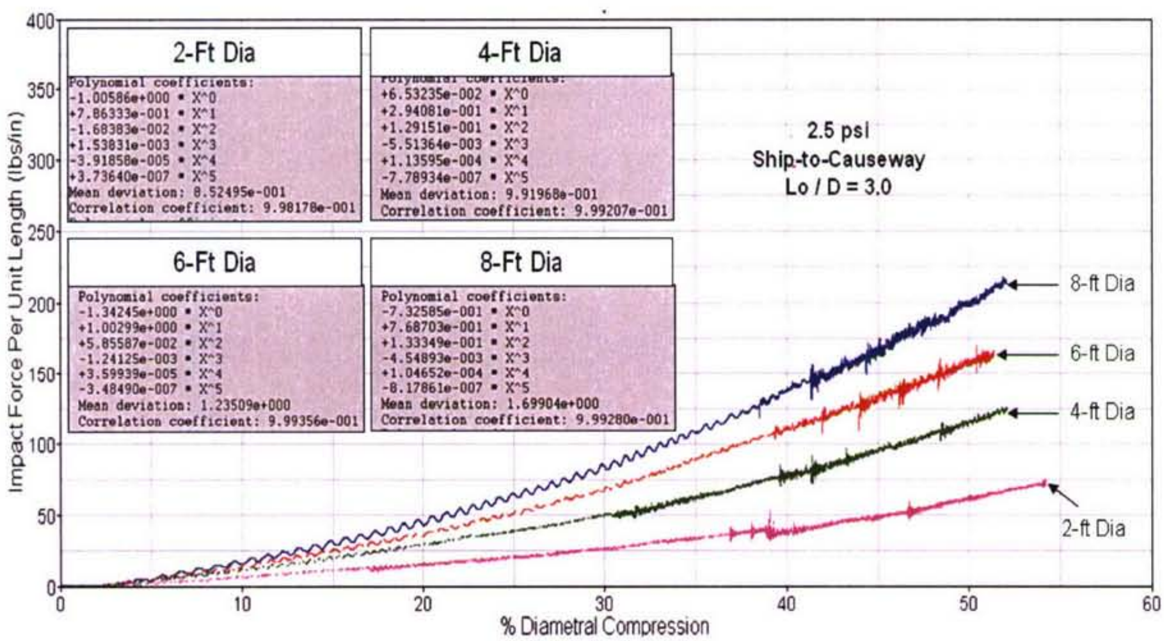

Figure 39. Impact Force per Unit Fender Length Versus Percent Diametral Compression Curves for Ship-to-Causeway Models at 2.5-psi Inflation Pressure

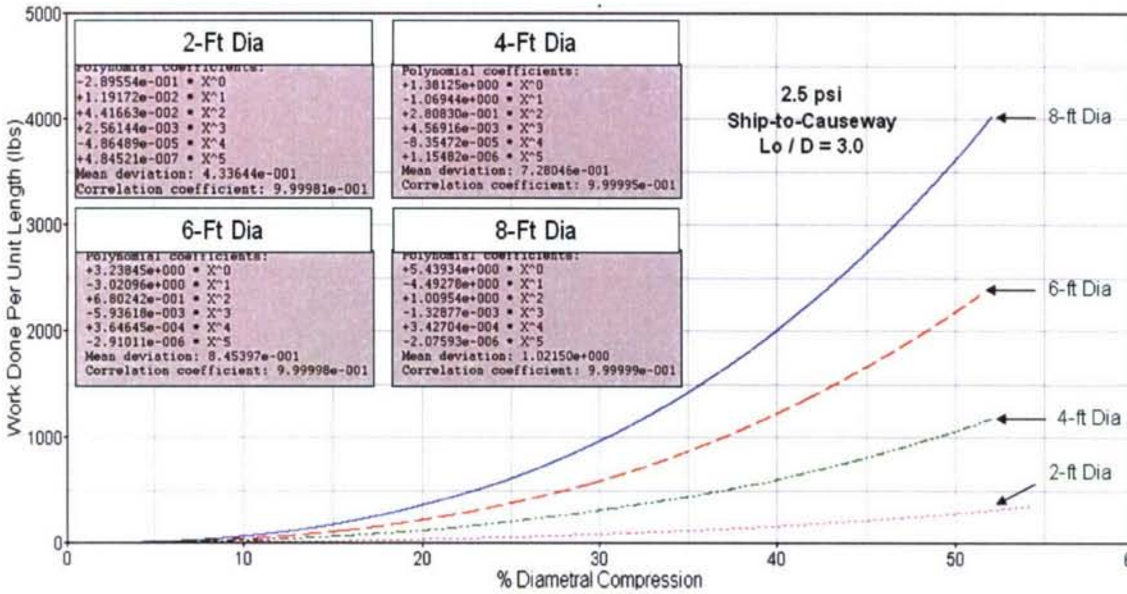

Figure 40. Work Done per Unit Fender Length Versus Percent Diametral Compression Curves for Ship-to-Causeway Models at 2.5-psi Inflation Pressure

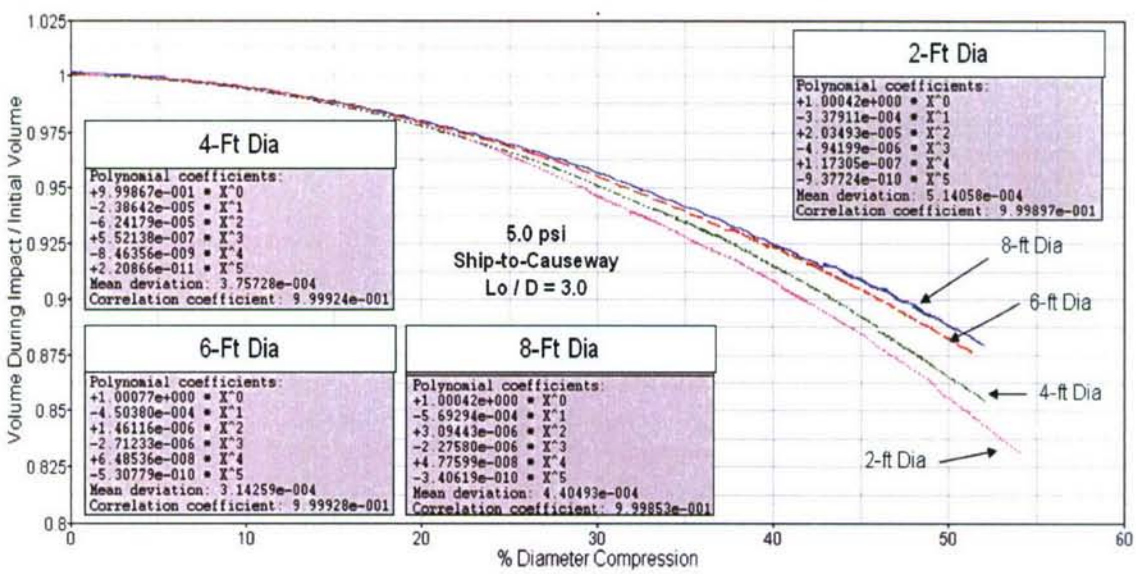

Figure 41. Normalized Volume Versus Percent Diametral Compression Curves for Ship-to-Causeway Models at 5.0-psi Inflation Pressure

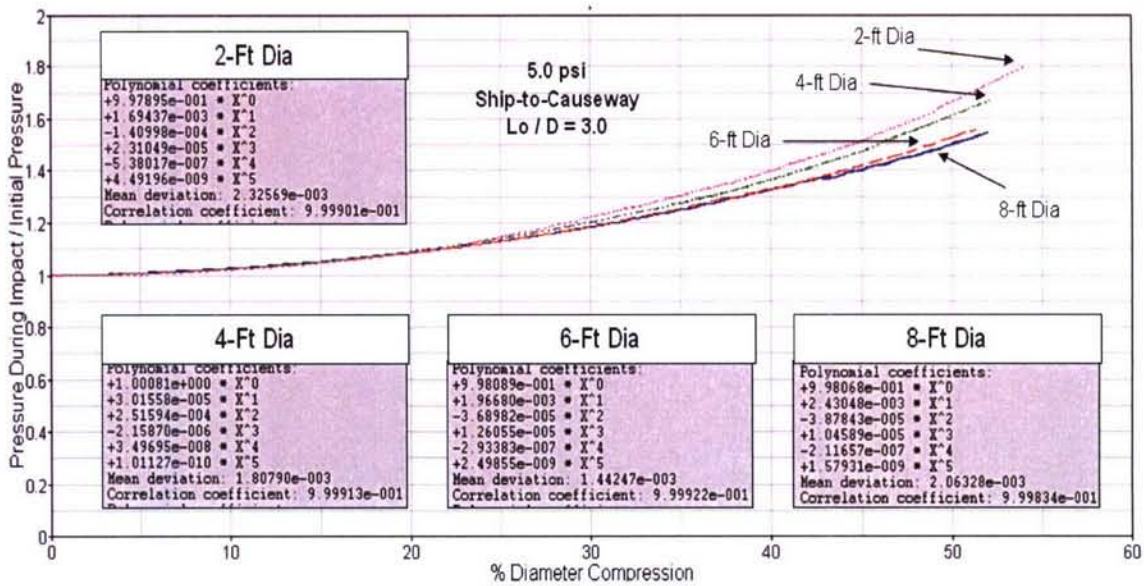

Figure 42. Normalized Pressure Versus Percent Diametral Compression Curves for Ship-to-Causeway Models at 5.0-psi Inflation Pressure

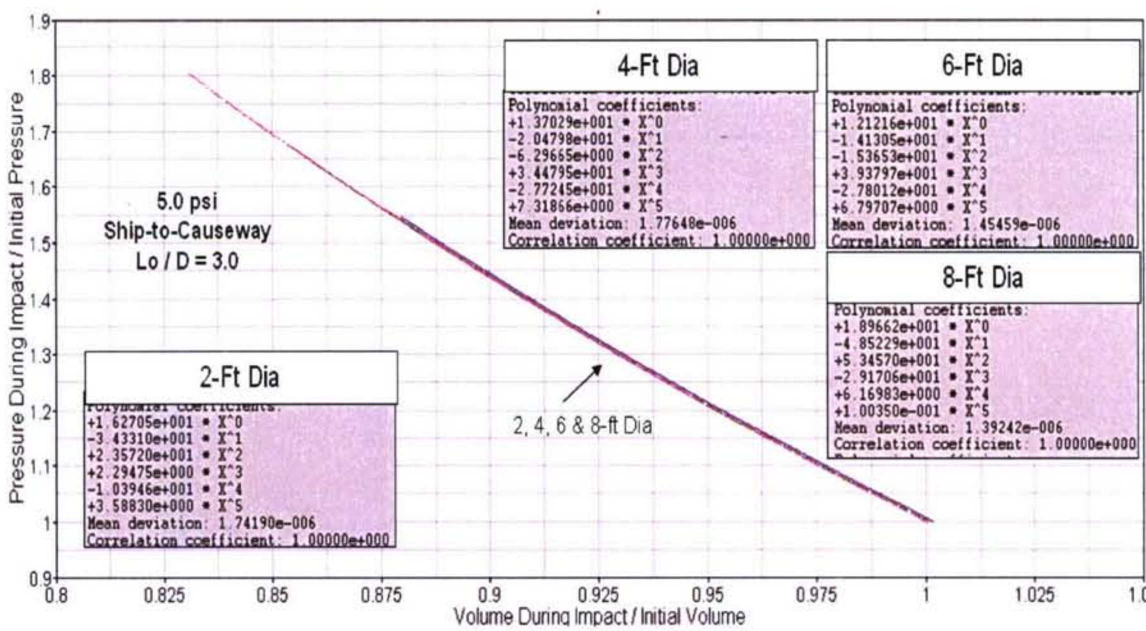

Figure 43. Normalized Pressure Versus Volume Curves for Ship-to-Causeway Models at 5.0-psi Inflation Pressure

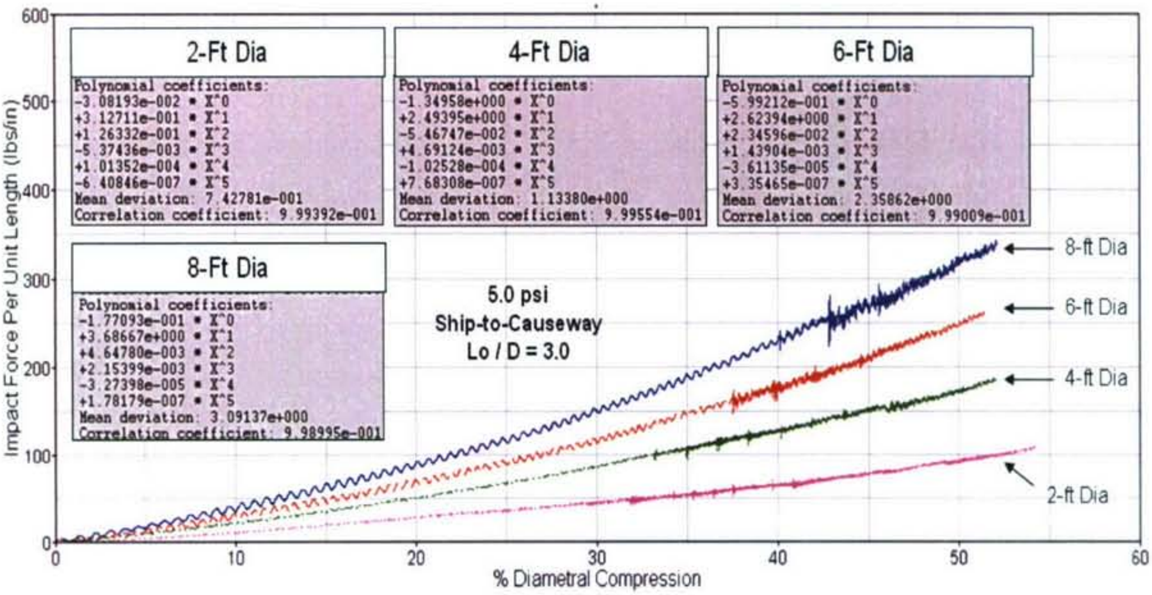

Figure 44. Impact Force per Unit Fender Length Versus Percent Diametral Compression Curves for Ship-to-Causeway Models at 5.0-psi Inflation Pressure

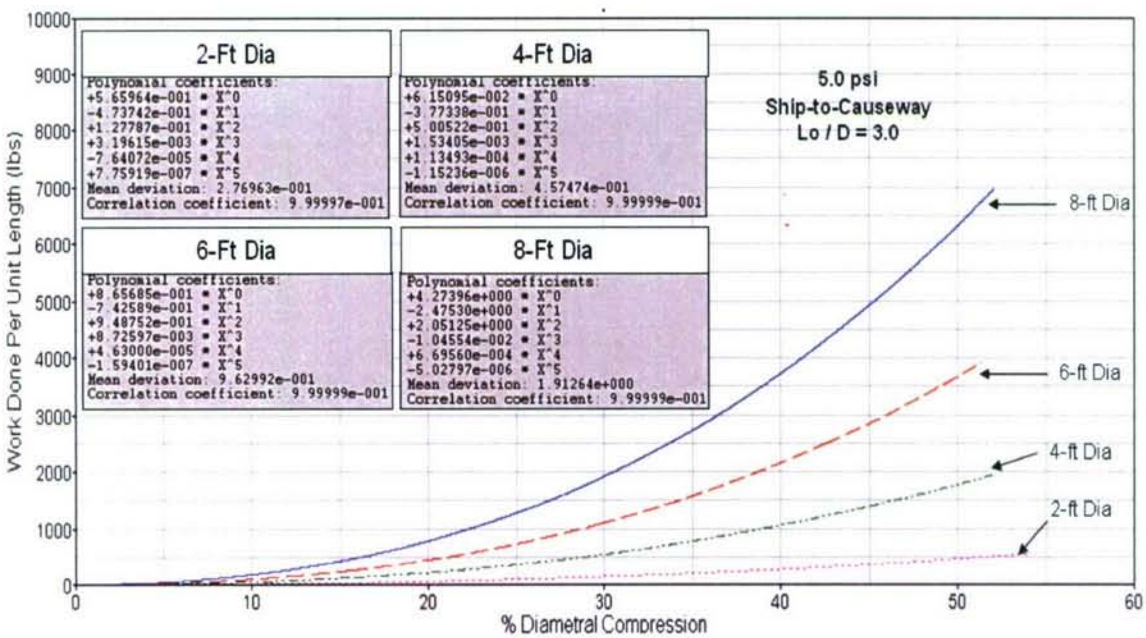

Figure 45. Work Done per Unit Fender Length Versus Percent Diametral Compression Curves for Ship-to-Causeway Models at 5.0-psi Inflation Pressure

Table 1. FEA Results of Ship-to-Ship Fender Models for 1.5-, 2.5-, and 5.0-psi Inflation Pressures and $(L_o/D) = 3.0$

Air Only Ship to Ship	Diameter [in]	Total Length [in]	Nominal Volume [in^3]	Total Weight [lb]	Initial Pressure [psi]	Pressurized Air Volume [in^3]	Difference Between Nominal & Pressurized Volumes [%]	Pressure At Max Impact [psi]	Impacted Air Volume [in^3]	Impact Displacement [in]	Impact Displacement [% Dia]	Impact Force [lb]	Integral Impact Force vs. Displacement [in-lb]	Integral PV (For Impact Only) [in-lb]	Strain Energy (During Impact Only) [in-lb]	Viscous Dissipation (During Impact Only) [in-lb]	Kinetic Energy (During Impact Only) [in-lb]	Wrinkling Observed? [Y/N]	Contribution of Kinetic Energy to Total External Work [%]	Contribution of Viscous Dissipation Energy to Total External Work [%]	Contribution of PV-Work to Total External Work [%]	Contribution of Strain Energy to Total External Work [%]
8 Ft. Dia 24 Ft Length	95.9	286.6	1,829,030	460	1.50	1,874,660	2.5%	6.06	1,462,860	50	52%	138,774	2,053,270	1,479,230	572,453	381	40	N	0.02	0.00	72.04	27.88
					2.50	1,906,370	4.2%	7.42	1,482,630	50	52%	167,214	2,658,350	2,013,780	642,383	243	25	N	0.01	0.00	75.75	24.16
					5.00	1,988,110	8.7%	10.95	1,526,910	50	52%	242,435	4,304,070	3,557,760	740,680	161	75	N	0.00	0.00	82.66	17.21
6 Ft. Dia 18 Ft Length	72.0	215.6	778,432	250	1.50	793,002	1.9%	6.27	612,702	37	51%	77,625	871,011	663,337	204,934	1,222	733	Y	0.14	0.08	76.16	23.53
					2.50	802,911	3.1%	7.36	626,122	37	51%	94,539	1,116,020	835,747	279,310	132	9	Y	0.01	0.00	74.89	25.03
					5.00	828,757	6.5%	10.74	641,759	37	51%	134,090	1,750,550	1,426,050	322,740	71	10	N	0.00	0.00	81.46	18.44
4 Ft. Dia 12 Ft Length	48.1	143.7	230,692	105	1.50	233,561	1.2%	6.83	175,764	25	52%	37,292	280,974	226,086	47,567	5,539	130	Y	1.97	0.05	80.47	16.93
					2.50	235,491	2.1%	8.12	177,479	25	52%	44,633	362,944	292,775	68,360	1,263	98	Y	0.35	0.03	80.67	18.83
					5.00	240,459	4.2%	11.08	183,774	25	52%	64,075	555,455	440,244	114,761	27	2	Y	0.00	0.00	79.26	20.66
2 Ft. Dia 6 Ft Length	24.0	71.9	28,837	28	1.50	29,016	0.6%	7.90	20,797	13	54%	11,025	41,310	35,733	3,963	1,169	11	Y	2.83	0.03	86.50	9.59
					2.50	29,135	1.0%	9.31	20,874	13	54%	12,870	53,005	45,650	5,140	1,713	18	Y	3.23	0.03	86.12	9.70
					5.00	29,436	2.1%	12.66	21,198	13	54%	17,875	81,487	69,284	9,831	1,806	8	Y	2.22	0.01	85.02	12.06

Table 2. FEA Results of Ship-to-Causeway Fender Models for 1.5-, 2.5-, and 5.0-psi Inflation Pressures and (L_o/D) = 3.0

Air Only Ship to Causeway	Diameter (in)	Total Length (in)	Nominal Volume (in^3)	Total Weight (lb)	Initial Pressure (psi)	Pressurized Air Volume (in^3)	Difference Between Nominal & Pressurized Volumes (%)	Pressure At Max Impact (psi)	Impacted Air Volume (in^3)	Impact Displacement (in)	Impact Displacement (% Dia)	Impact Force (lb)	Integral Impact Force vs. Displacement (in-lb)	Integral PV (For Impact Only) (in-lb)	Strain Energy (During Impact Only) (in-lb)	Viscous Dissipation (During Impact Only) (in-lb)	Kinetic Energy (During Impact Only) (in-lb)	Wrinkling Observed? (Y/N)	Contribution of Kinetic Energy to Total External Work (%)	Contribution of Viscous Dissipation Energy to Total External Work (%)	Contribution of PV-Work to Total External Work (%)	Contribution of Strain Energy to Total External Work (%)
8 Ft. Dia 24 Ft Length	95.9	286.6	1,829,030	460	1.50	1,874,660	2.5%	3.79	1,642,320	50	52%	46,413	837,532	603,313	203,813	17,500	3,593	Y	2.09	0.43	72.03	24.33
					2.50	1,906,370	4.2%	4.89	1,674,020	50	52%	61,883	1,169,950	845,683	293,615	17,870	2,300	Y	1.53	0.20	72.28	25.10
					5.00	1,991,130	8.9%	7.73	174,845	50	52%	98,077	2,025,600	1,530,850	434,870	35,457	3,479	Y	1.75	0.17	75.58	21.47
6 Ft. Dia 18 Ft Length	72.0	215.6	778,432	250	1.50	793,002	1.9%	3.92	690,041	37	51%	27,795	361,860	273,102	70,041	11,943	1,379	Y	3.30	0.38	75.47	19.36
					2.50	802,911	3.1%	5.04	699,599	37	51%	35,045	508,329	383,698	109,142	8,683	1,698	Y	1.71	0.33	75.48	21.47
					5.00	828,757	6.5%	7.80	725,900	37	51%	56,998	855,450	653,692	181,184	12,507	539	Y	1.46	0.06	76.41	21.18
4 Ft. Dia 12 Ft Length	48.1	143.7	230,692	105	1.50	233,561	1.2%	4.36	198,511	25	52%	14,385	126,260	99,996	20,050	4,470	191	Y	3.54	0.15	79.20	15.88
					2.50	235,491	2.1%	5.49	200,647	25	52%	18,123	170,440	136,378	26,080	5,294	523	Y	3.11	0.31	80.02	15.30
					5.00	240,468	4.2%	8.36	205,500	25	52%	27,116	282,521	230,386	45,178	4,768	156	Y	1.69	0.06	81.55	15.99
2 Ft. Dia 6 Ft Length	24.0	71.9	28,837	28	1.50	29,016	0.6%	4.90	23,982	13	54%	4,179	19,062	15,568	1,869	1,239	30	Y	6.50	0.16	81.67	9.80
					2.50	29,135	1.0%	6.04	24,167	13	54%	5,069	24,848	20,661	2,498	1,218	72	Y	4.90	0.29	83.15	10.05
					5.00	29,436	2.1%	9.01	24,453	13	54%	7,825	40,499	34,303	4,405	1,320	10	Y	3.26	0.03	84.70	10.88

Tables 1 and 2 indicate that E_{strain_energy} was an appreciable percentage of external work done—as much as 27.88% for the ship-to-ship case and 25.10% for the ship-to-causeway case; however, as volume changes caused by impact became increasingly larger, the contribution of E_{strain_energy} as a percentage of total work done decreased. Furthermore, although the data are limited, E_{strain_energy} was observed to decrease with increasing volume and pressure for nonwrinkled fenders.

FEA modeling results clearly showed that the effects of material extensibility were caused from the strain energies developed in the fabric layer. Although the analytical solution described in the appendix invoked the assumption of inextensible fabric behavior, volume changes attributed to initial inflation pressures were not admissible. FEA modeling revealed relationships between changes in diameter versus initial inflation pressures (pressure at the end of step 1) (see figure 46). Tables 1 and 2 list the percent differences between the nominal and initially pressurized fender volumes, the largest of which was 8.7% for the 8-foot-diameter DAFS fender inflated to 5.0 psi.

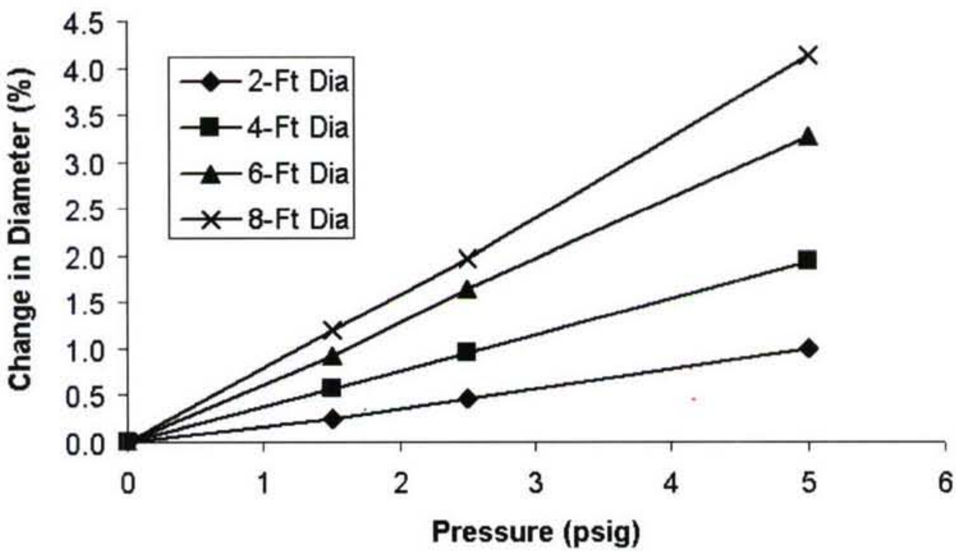

Figure 46. Effect of Material Extensibility on the FEA Diameter-Pressure Behavior for Ship-to-Ship Models

Reference 1 successfully validated numerical model predictions against experimental results for an air beam subjected to lateral compression; it further investigated the effects of material stiffness on fender compressibility for an order of magnitude range of linear elastic moduli (E = 0.1 Mpsi to 1.0 Mpsi). It was established that, for membrane fenders and this range of elastic moduli at equal diametral compression, no appreciable effects on contact force, total work done, and *PV-work* resulted. As the strain energy decreased with increasing elastic modulus, however, stresses within the fabric increased as expected.

This study evaluated the energy absorption behavior of different diameter DAFS fenders subject to quasi-static, ship-to-ship and ship-to-causeway (figures 12 through 15) mooring configurations. Transient effects, however, were evident in the graphs of tracked results (figures 8 through 11 for ship-to-ship and figures 12 through 15 for ship-to-causeway).

These transients were shown to negligibly influence the energy balance of equation (1). The ABAQUS/Explicit FEA code is primarily used for dynamic problems involving highly transient phenomena, such as shock and blast events, and is especially suited for structural problems experiencing significant nonlinearities and extensive contact interactions including self-contact caused by wrinkling. Because this code uses an explicit time-integration scheme and does not require inversion of the global stiffness matrix, the solver is much faster than implicit FEA solvers. The number of time increments required by an explicit solver, however, can easily exceed that of implicit solvers by several orders of magnitude. Solutions for static and quasi-static problems require considerable loading times to prevent exciting dynamic modes. Although the time intervals used to inflate and impact the fender models were kept intentionally small for computational efficiencies and, though the 1.0-second inflation time may not be realistic, especially for large DAFS fenders, the resulting maximum values of $E_{kinetic\_energy}$ and $E_{dissipation\_energy}$ were negligible (< 3.3% for all models) in comparison to the external work. The energy absorption attributed to impact is simply the work done by external forces, which is also the change in $E_{internal\_energy}$ between the inflated and impacted states.

SCALABILITY OF ENERGY ABSORPTION RESULTS

Scalability of the FEA-predicted energy absorption results shown in tables 1 and 2 with respect to volumes must consider either the external work done, $\int F\,d\delta$, or $E_{internal\_energy}$, and not just the *PV-work*. Because the FEA solution involves multiple energy paths within the fender and must necessarily include the elasticity effects of the fabric, scaling the *PV-work* without consideration of E_{strain_energy} (and $E_{kinetic\_energy}$ and $E_{dissipation\_energy}$ in dynamic analyses) will yield misleading results. Equation (5) relates the external work done to different fender volumes and is valid only when the pressure conditions shown below are satisfied:

$$\left(\int F d\delta\right)_{LARGE} = \frac{V_{LARGE}}{V_{SMALL}}\left(\int F d\delta\right)_{SMALL}, \qquad (5)$$

when $P_{abs\_initial\_large} = P_{abs\_initial\_small}$ and $P_{abs\_final\_large} = P_{abs\_final\_small}$, where P_{abs} is absolute pressure.

It should be noted that when these conditions are met, the percent-diametral compressions of the fenders being compared might not be necessarily equal. Furthermore, fabric wrinkling during compression produces additional volume reductions that will affect scalability.

CONCLUSIONS

This research established performance curves detailing the energy absorption parameters of selectively sized DAFSs. Numerical solutions were generated using the ABAQUS/Explicit FEA program for two mooring configurations: ship-to-ship and ship-to-causeway (non-ballasted). The governing energy balance was presented, and the contributions of strain energy and *PV-work* were assessed for various inflation pressures and DAFS sizes. The applicability and limitations of analytical methods based on assumptions of material inextensibility were also discussed. Comparisons were made between the numerical and analytical methods to demonstrate the importance of admitting strain energies of the fender material in the energy balance. Equations and conditions for proper scaling of pressure and volume terms in energy absorption calculations were developed and discussed. The results of this research will enable future efficiencies in fender design and expand the applicability of DAFS fenders to vessels beyond the JHSV.

REFERENCES

1. C. Quigley, K. Buehler, P. Cavallaro, and D. Jacobson, "Deployable Air Beam Fender System – Phase-I Report," Natick Soldier Center, Natick, MA, 2005.

2. *ABAQUS/Explicit Finite Element Analysis Program, Version 6.4*, ABAQUS Inc., Pawtucket, RI, 2004.

APPENDIX
ANALYTICAL SOLUTION OF FENDER ENERGY ABSORPTION

This analysis simulates the 8-Ft DAFS Fender FEA model subject to ship-to-ship (air only) impact. The inputs of diameter, pressures, initial volume and displacement used here match those of this specific FEA model. This analysis is only valid for full length contact as provided by the ship-to-ship condition because of the necessary assumptions used in the displacement-deformation relationship.

$D := 95.71 \qquad V_{initial} := 1988110 \qquad \delta := 50$

$P_A := 14.7 \qquad P_{initial} := 5 \qquad P_{final} := 10.95$

$P_{abs\_initial} := P_{initial} + P_A \qquad P_{abs\_initial} = 19.7 \qquad P_{abs\_final} := P_{final} + P_A \qquad P_{abs\_final} = 25.65$

$V_{final} := \dfrac{P_{abs\_initial} \cdot V_{initial}}{P_{abs\_final}} \qquad V_{final} = 1.527 \times 10^6$

Define volume as a range variable and compute absolute pressure using the volume range variable and the Ideal Gas Law for adiabatic conditions:

$V := V_{final}, 1.0001 \cdot V_{final} .. V_{initial} \qquad P_{abs}(V) := \dfrac{P_{abs\_initial} \cdot V_{initial}}{V} \qquad P_{gage}(V) := P_{abs}(V) - P_A$

$P_{abs}(V_{final}) = 25.65 \qquad P_{abs}(V_{initial}) = 19.7$

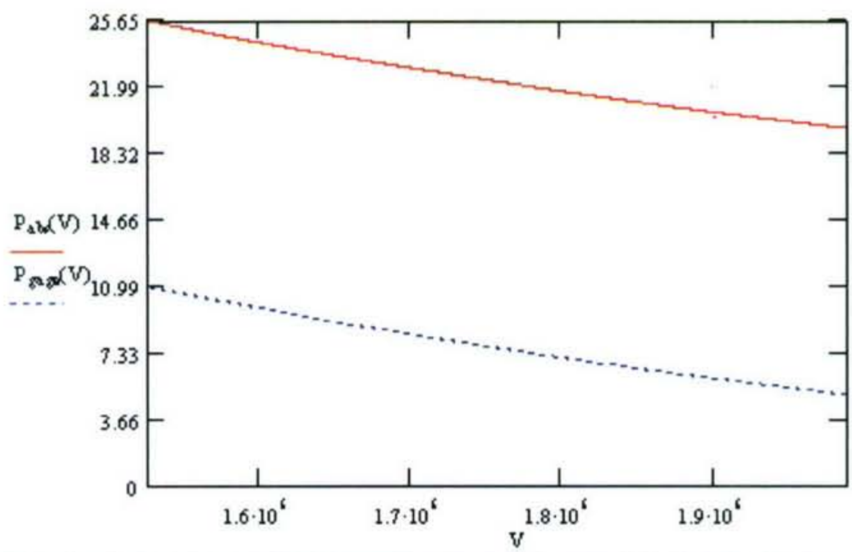

Compute work done on the air using gage pressure. (For a flexible pressure vessel exposed to external ambient pressure, the ambient pressure does work that must be subtracted which is automatically done if the gage pressure is used as shown.)

$$\text{Work} := -\left[\int_{V_{initial}}^{V_{final}} \left(P_{abs}(V)\right) dV - \int_{V_{initial}}^{V_{final}} P_A\, dV\right] \qquad \text{Work} = 3.557 \times 10^{6}$$

For an inextensible membrane, the circumference is constant during impact so the following expression relates the original circular diameter, D, to the radius of the deformed cross section, r, and the width of each of the 2 flat contacting sections, Wcontact:

$$r := \frac{D - \delta}{2} \qquad r = 22.855$$

$$W_{contact} := \frac{\pi}{2}\cdot(D - 2r) \qquad W_{contact} = 78.54$$

CHECK:

$$\pi\cdot D = 300.682$$

$$2\pi\cdot r + 2W_{contact} = 300.682$$

Using conservation of perimeter along the length axis, express the length of each of the 2 flat contacting sections, Lcontact, in terms of the radius of the deformed volume, r:

First, compute the length of the straight cylindrical section of the fender from the known initial volume:

$$L_{cylinder} := \frac{4}{\pi\cdot D^2}\cdot\left[V_{initial} - \frac{4}{3}\cdot\pi\cdot\left(\frac{D}{2}\right)^3\right] \qquad L_{cylinder} = 212.528$$

$$L_{contact} := \pi\cdot\left(\frac{D}{2} - r\right) + L_{cylinder} \qquad L_{contact} = 291.068$$

CHECK:

$$\pi\cdot D + 2\cdot L_{cylinder} = 725.739$$

$$2\cdot\pi\cdot r + 2\cdot L_{contact} = 725.739$$

Compute contact area, impact force and express work done in units of ft-lbs:

$$\text{Area}_{contact} := L_{contact}\cdot W_{contact} \qquad \text{Area}_{contact} = 2.286 \times 10^{4}$$

$$F := P_{gage}\left(V_{final}\right)\cdot \text{Area}_{contact} \qquad F = 2.503 \times 10^{5}$$

$$\text{Work}_{ft\_lbs} := \frac{\text{Work}}{12000} \qquad \text{Work}_{ft\_lbs} = 296.457$$

INITIAL DISTRIBUTION LIST

Addressee	No.
Office of Naval Research (ONR-334 (R. Barsoum))	1
U.S. Army Natick Soldier Center (C. Quigley)	5
Army Research Laboratory, Langley (MS-188E (A. R. Johnson))	1
Army Research Laboratory, Aberdeen (AMSRL-WM-MB (R. Dooley, B. Cheeseman, D. Granville))	3
The City College of New York, New York, NY (A. Sadegh)	1
Defense Technical Information Center	2
Center for Naval Analyses	1